Results in Atmospheric Waves

By

Arthur J. Kalb

DISSERTATION

Submitted in partial satisfaction of the requirements for the degree of

DOCTOR OF PHILOSOPHY

in

APPLIED MATHEMATICS

in the

OFFICE OF GRADUATE STUDIES

of the

UNIVERSITY OF CALIFORNIA

DAVIS

Approved:

Joseph A. Biello

John K. Hunter

Terry R. Nathan

Committee in Charge

2024

To Vivian

Contents

Abstract

In the first chapter, we extend previous analysis of dissipative modes derived using a wave radiation boundary condition at the tropopause by considering the effects of relaxing hydrostatic balance, finding agreement in the hydrostatic limit. The absence of hydrostatic balance on shorter horizontal length scales introduces a singular perturbation of the problem which corresponds to the emergence of a novel barotropic mode. The frequency of this barotropic mode provides a limit to the frequency and decay rate of the high horizontal wavenumber baroclinic modes, thereby introducing a scale selective wave drag. The decay of the baroclinic modes can be characterized by the angle of the wavefront. A damping operator for the bulk equations is proposed, so that the damped rigid lid solutions approximate this decay.

In the second chapter, we investigate the effect of restricting the sign of the phase velocity of waves with small wavenumber, nonzero frequency and dispersion in one spatial dimension using multiscale asymptotics. We consider two examples of long waves with these characteristics. The first investigates breather solutions to the Sine-Gordon equation used in quantum field theory. The second considers the Yanai wave observed in the equatorial atmosphere. Ultimately, we find that this restriction of direction changes the description of the waves in a subtle way, but does not produce any new physics.

In the the third chapter, we investigate the effects of meridional circulation on the equatorial waves. We find that relaxing the long wave scaling used in previous work no longer guarantees stability, and find a necessary condition for instability.

In the fourth chapter, we investigate the effects of a zonally moving off-equatorial forcing on equatorial waves. We find a formula that describes the magnitude of a Kelvin response, as well as a mechanism for such excitations via the interaction of barotropic and baroclinic waves.

Acknowledgments

I have many whom I would like to thank in their contributions to this dissertation.

Firstly, I would like to thank those who contributed in tangible ways either by teaching or by discussions with me. First among these is Dr. J. Biello for serving as my advisor for five years as I worked through this, providing direction and insight into this research. To those who served on my committees: Drs. J. Hunter, T. Nathan, B. Thomases, and D. Yang. To those professors: Drs. M. and A. Igel, E. Goldsmith, D. Marsico, and to fellow students: O. Koul, D. Falcone, C. Zheng, K. Brown, G. Pandya, T. Greiner, and W. Niu for their lessons and discussions as I worked through this. I would also like to thank to the reviewers any and all papers that may come out from this for their work.

Next, to those who contributed in less tangible ways, mostly for their love and support. First among these is my lovely wife Vivian, whom I could not thank enough. To my parents, Art and Margaret, my parents-in-law, Linda and Mike, my siblings and siblings-in-law: JP, Marie, Joe, Tommy, Theresa, Patricia, Ed, Andy, Matt, Ginny and Otto. To all of my relatives, especially to Lucy and Sheila, who passed away during my studies. Finally to my friends: Wenjun and Catherine, Kyle and Emily, Cameron, Diogo, Joey, both Patrick's, Priscilla, Josh, Andrea, Jerome, Michael, Natalie, Dana, Eric and many more.

CHAPTER 1

Leaky Rigid Lid Tropospheric Modes in a Nonhydrostatic Atmosphere

1.1. Introduction

Tropospheric dynamics is often modeled using a framework whose vertical structure is described by a set of discrete modes [**Majda, 2003**, **Khouider et al., 2012**]. This convenient approximation restricts convective or dynamical models entirely to the troposphere, whose finite vertical extent has a discrete spectrum with normal boundary conditions. A finite troposphere is most commonly modeled via the rigid lid boundary conditions, in which the vertical velocity vanishes at the tropopause.

In this context, the first justification for the rigid lid boundary condition is that free surface perturbations at the tropopause are often of much smaller amplitude than those within the troposphere, especially when perturbations arise from convective activity. This was demonstrated in Franklin's oil and water experiment [**Franklin, 1905**], and observed naturally in instances like the dead water phenomena, where a strong salinity gradient prevents mixing between two layers of water [**Ekman, 1904**]. This argument is often used on material of drastically different density, such as the atmosphere and the ground, which we readily accept. The second justification for using a rigid lid condition is that the stratosphere has a stronger stratification than the troposphere, which inhibits vertical motion, and this justification is commonly used at the tropopause. This assumption is often presented mathematically by stating that the ratio between stratospheric and tropospheric stratification is infinite.

However, there are several objections to the use of rigid lid boundary conditions. Firstly, the real atmosphere is closer to a semi-infinite domain, and so is more prone to have a continuous spectrum of modes. Consequently, [**Lindzen, 2003**] argues that discrete internal modes that are observed are incorrectly based on oversimplified models. By contrast, he claims that the atmosphere "is characterized by a single isolated eigenmode and a continuous spectrum", and then proceeds

to provide arguments for the observed properties, such as the observed equivalent depths, are consistent such a setup.

Despite this objection, the rigid lid framework is a ubiquitous assumption in simplified and analytical models of tropospheric dynamics. Models of tropical wave dynamics, which have been successful at describing convectively coupled equatorial waves [**Matsuno, 1966**,**Gill, 1980**,**Neelin and Held, 1987**, **Kiladis et al., 2009**, **Biello and Majda, 2004**] often project the primitive equations onto the shallow water modes for the first few rigid lid baroclinic modes, yielding a system of coupled shallow water equations. It has also been used to introduce moist dynamics in the atmosphere using only the first two baroclinic modes with minimal vertical information [**Majda and Shefter, 2001**, **Khouider and Majda, 2006**]. One process these models must incorporate into their derivation is how internal gravity waves lose energy over time. A common strategy is to introduce Newtonian cooling or radiative damping on a scale of 1-10 days [**Matsuno, 1966**, **Gill, 1980**], though often it is modelled as being stronger than observation would suggest [**Battisti et al., 1999**]. Another strategy in a finite domain is to impose a wave radiation boundary condition at the tropopause to allow all internal gravity waves to leave the domain [**Bennett, 1976**, **Klemp and Durran, 1983**,**Garner, 1986**,**Purser and Kar, 2002**]. However, these boundary conditions are derived by using the dispersion relation of rigid lid modes to filter out the outgoing waves, rather than being grounded in some physical mechanism.

Another objection to the use of the rigid lid is that the stratification ratio is close to 2, which is not large enough to unambiguously justify the approximation. In light of this, [**Chumakova et al., 2013**] (henceforth CRT) and [**Edman and Romps, 2017**] (henceforth ER) both assume this finite stratification and derive a discrete spectrum of internal gravity waves. Both find that the waves decay in time without having to artificially impose Rayleigh friction, Newtonian cooling, or wave filtering. While both use the common assumption of a finite stratification ratio, they begin with a slightly different set of assumptions that are relevant in their respective analyses and conclusions. [**Lin and Emanuel, 2022**, **Yano and Emanuel, 1991**] also consider the damping effects of stratospheric coupling, however both simplify the vertical structure of the problem and as such differ significantly in the analysis of CRT and ER.

CRT approaches the problem by assuming an incompressible, hydrostatic atmosphere with a vertical density profile that is prescribed by a piecewise constant Brunt-Väisälä frequency, N^2.

The strong gradient in N^2 is used to find a jump condition in kinetic energy density. This jump condition is reformulated as an effective boundary condition that allows for upward wave radiation of waves from the troposphere, restricting attention to the troposphere alone. A boundary value problem is then solved to find the discrete spectrum, which includes decay rates proportional to the horizontal wavenumber.

ER attempts to generalize upon this work by considering a similar setup, but assumes a Boussinesq two layer atmosphere, which has a constant vertical density profile, except when computing N^2. They consider the effect of a buoyancy source in the troposphere and are able to find a Green's function response to that source in both the troposphere and stratosphere. As such, due to the Boussinesq assumption, there is no jump condition at the tropopause coming from the gradient in N^2. This distinction is important to recall when comparing the two analyses.

The primary objective of this manuscript is to relax the hydrostatic assumption taken in CRT and find the equivalent leaky modes of the troposhere, in an effort to better understand the structure of these modes at shorter horizontal length scales, as would be appropriate for internal waves generated by convective activity, such as in recent work by [**Marsico et al., 2023**], which uses a parameterized drag. We study the linear equations appropriate to the troposphere in the presence of a discontinuous Brunt Vaisala frequency at the tropopause, finding a boundary condition that is consistent with CRT, but presents problems in the analysis. We find modes that are analogous to the leaky modes computed by CRT, but nonhydrostatic flow introduces a new barotropic mode. The frequency of this barotropic mode serves as a limit to the frequencies and decay rates of the baroclinic modes for large horizontal wavenumbers. What results is the decay rate increases with angle of elevation (defined via a ratio of horizontal and vertical wavenumbers) until a critical angle of about 60°, above which the decay rate decreases.

The paper is organized as follows: Section 2 introduces the main equations and the jump condition, which produce an eigenvalue problem in Section 3. Section 4 discusses the eigenfunctions of the problem. Section 5 discusses how this decay can be approximated via an empirically derived operator.

1.2. Derivation and boundary conditions

We begin with linearized incompressible, nonrotating, non-hydrostatic fluid equations in one vertical and one horizontal dimension, like in CRT,

$$\begin{aligned} \rho_0 u_t + p_x &= 0, \\ \rho_0 w_t + p_z + g\rho &= 0, \\ \rho_t + \rho_{0z} w &= 0, \text{ and} \\ u_x + w_z &= 0. \end{aligned} \tag{1.1}$$

Here we define x, z and u, w as the horizontal and vertical coordinates and velocities respectively, p, ρ as the pressure and density perturbations from $p_0(z), \rho_0(z)$, and g is the gravity constant. We also impose the rigid lid boundary condition $w(z = 0) = 0$ for the ground. Letting $N^2 = -g\rho_{0z}/\rho_0$, we can reduce the system to a single equation

$$\frac{(\rho_0 w_z)_{ztt}}{\rho_0} + w_{xxtt} + N^2 w_{xx} = 0. \tag{1.2}$$

This equation uses the same manipulations of (1) in CRT, and the w_{xxtt} term arises from the vertical acceleration term. Here the structure of ρ_0 plays an important role. If it is constant, then the density cancels in the numerator and denominator to yield something akin to equation (7) in ER. If we specify only that the atmosphere is incompressible like in CRT, then the structure of $\rho_0(z)$ becomes important and it can be computed via the Brunt-Väisälä (B-V) frequency $N^2(z)$. To make sure that the structure of $\rho_0(z)$ does not obfuscate our findings, the more physically significant kinetic energy density $\phi^2 = \rho_0 w^2$ is used instead of w [**Raupp et al., 2019**, **Kasahara and Qian, 2000**]. Therefore we substitute $\phi = \sqrt{\rho_0} w$ to get

$$\phi_{zztt} + \left(\frac{-N^4}{4g^2} + \frac{1}{2g} \frac{dN^2}{dz} \right) \phi_{tt} + \phi_{xxtt} + N^2 \phi_{xx} = 0. \tag{1.3}$$

We nondimensionalize this equation using a typical depth of the troposphere $\tilde{H}$, which sets the location of the tropopause to $z = 1$, a tropospheric reference value for the buoyancy frequency $\tilde{N}$, and the ratio of the vertical to horizontal length scales δ. From it emerges the time scale $\tilde{t} = (\delta \tilde{N})^{-1}$, and velocity scales $\tilde{w} = \tilde{H}/\tilde{t}, \tilde{u} = \tilde{w}/\delta$. We also see the nondimensional parameter $\epsilon = \tilde{N}\tilde{H}/\sqrt{2g\tilde{H}}$ emerge as a ratio between the height of the troposphere and the height scale of density. In total,

nondimensionalization of the equation yields

$$\phi_{zztt} + \left(-\epsilon^4 N^4 + \epsilon^2 \frac{dN^2}{dz}\right)\phi_{tt} + \delta^2 \phi_{xxtt} + N^2(z)\phi_{xx} = 0. \tag{1.4}$$

For the atmosphere described in CRT, $\delta = 0.016, \epsilon^2 = 0.082$, and they consider the limits with both vanishing. We still use ϵ vanishing, but in contrast we also take that $\delta = \tilde{H}/\tilde{L} = 1$, approximately on the scale of a single thunderstorm. It will also be shown in Section 3, via rescaling of the frequency and horizontal wavenumber that any nonzero δ can always be scaled to 1, i.e. our horizontal wavenumbers can always be scaled to match the vertical wavenumbers. CRT describes the $\delta = 0$ case, and we call the limiting case of $\delta \to 0$ the hydrostatic limit. Since the tropospheric B-V frequency is used as our time scale, the stratospheric B-V frequency is denoted N_2. We integrate vertically and in time to compute the jump conditions at the tropopause, where it is assumed that $N^2(z)$ has a jump discontinuity

$$[\phi] = 0, \quad [\phi_z] + \epsilon^2 [N^2(z)]\phi = 0, \tag{1.5}$$

where $[\cdot]$ captures the difference across the two sides of the layer $z = 1$. This is equivalent to a trivial jump condition, obtained by unpacking the definition of ϕ,

$$[w] = 0, [w_z] = 0. \tag{1.6}$$

In short, the scaling and limits produces in the following system of equations

$$\begin{aligned} \phi_{zztt} + \phi_{xxtt} + \phi_{xx} &= 0, \quad 0 < z < 1, \\ \phi_{zztt} + \phi_{xxtt} + N_2^2 \phi_{xx} &= 0, \quad z > 1, \\ [\phi] = 0, [\phi_z] &= 0, \quad \text{at } z = 1, \text{ and} \\ \phi &= 0, \quad \text{at } z = 0. \end{aligned} \tag{1.7}$$

1.3. Finding the modes

Our next objective is to find a condition which identifies tropospheric modes in (1.7). The tropopause has been temporarily set to $z = 0$. The terms in our solution are defined with respect to the troposphere, we have a incoming (I), reflected (R), and transmitted (T) terms. We assume the same radiative condition as CRT that there is no incoming stratopsheric terms, producing the

similar

$$\phi_I = \exp\left(ikx + \lambda t + \frac{|k|}{\lambda}\sqrt{1+\lambda^2}z\right),$$
$$\phi_R = R\exp\left(ikx + \lambda t - \frac{|k|}{\lambda}\sqrt{1+\lambda^2}z\right), \text{ and}$$
$$\phi_T = T\exp\left(ikx + \lambda t + \frac{|k|}{\lambda}\sqrt{N_2^2+\lambda^2}z\right). \tag{1.8}$$

Continuity ensures that k, λ will not differ across the tropopause. The vertical wavenumbers above come from the dispersion relation

$$\lambda^2 = \frac{N^2k^2}{m^2-k^2}, \tag{1.9}$$

with the signs matching the $\delta = 0$ case covered by CRT. We note that while k is real, λ is complex, which complicates our analysis. Since energy can leave the troposphere but not enter it, this implies that the real part of $\lambda \leq 0$, generally resulting in decaying modes. This allows us to define the branch of the square root term $s_a(\lambda;\delta) := \sqrt{a^2+\delta^2\lambda^2}$ by setting $s(0;\delta) = s(\lambda;0) = a$, with branch cuts going in a semi-circular arc between the branch points $\lambda = \pm ia$ via the positive real half plane. This choice of branch allows for agreement with CRT in the hydrostatic limit. In a similar fashion we implicitly defined above $\sqrt{\lambda^2} = \lambda$ to get the vertical wavenumbers, with that branch cut on the positive real axis. The jump conditions in this setup are

$$T = 1 + R$$
$$\frac{|k|}{\lambda}Ts_{N_2}(\lambda;\delta) = \frac{|k|}{\lambda}s_1(\lambda;\delta)(1-R). \tag{1.10}$$

By substituting the first into the second, we can simplify this in terms of the tropospheric terms alone to obtain

$$s_{N_2}(\lambda;\delta)H(\phi_x) = -\phi_{zt}. \tag{1.11}$$

where $H[e^{ikx}] = -i\text{sign}(k)e^{ikx}$ is the Hilbert transform. The $s_{N_2}(\lambda;\delta)$ operator is new, but is to be an extension of the Bochner-Riesz operator S [**Stein and Murphy, 1993**], where

$$N_2S[e^{i\omega t}] = \sqrt{N_2^2-\omega^2}e^{i\omega t} \tag{1.12}$$

from the real frequencies to the whole complex plane $\lambda = \mu + i\omega$. Proper use of the Bochner-Riesz operator on a function requires a Fourier inversion integral over all frequencies $|\omega| < N$, which requires a full temporal knowledge of the modes, even before considering our extension. This renders it incompatible with any attempt to solve an initial value problem.

While we are unable to set up, let alone solve, the differential equation as an initial value problem, an examination of the modes produced by this boundary condition is still physically illuminating. Returning to our original vertical coordinate, and using the rigid lid lower boundary condition and the tropospheric differential equation, we find that the tropospheric terms ϕ_I, ϕ_R sum up to

$$\phi = \sinh\left(\frac{kz}{\lambda} s_1(\lambda;\delta)\right) \exp(ikx + \lambda t),$$

which when substituted into (1.11) produces

$$\sqrt{N_2^2 + \lambda^2}\sinh\left(\frac{|k|}{\lambda} s_1(\lambda;\delta)\right) + \sqrt{1+\lambda^2}\cosh\left(\frac{|k|}{\lambda} s_1(\lambda;\delta)\right) = 0 \tag{1.13}$$

$$\text{OR } \tanh\left(\frac{|k|}{\lambda} s_1(\lambda;\delta)\right) = -\frac{s_1(\lambda;\delta)}{s_{N_2}(\lambda;\delta)}. \tag{1.14}$$

The latter expression reduces to the condition found by CRT in the hydrostatic limit $\delta \to 0$. As $\lambda \to 0$, it also reduces to the CRT condition up to $O(\lambda^2)$, and as such both have an accumulation point at $\lambda = 0$. Since (1.13) is analytic except at $\lambda = 0, \pm i, \pm iN_2$ or along the branch cuts, there will be only a finite number of zeros in any bounded domain that avoids these. Additionally, we observe that we can define $\Lambda = \delta\lambda, \kappa = \delta k$ for any nonzero δ, which allows for us to choose $\delta = 1$ without loss of generality.

Solutions to Equation (1.13,1.14) in the complex plane were found numerically, with no difference between the two. The complex square root terms were defined such that the above branches satisfy the same conditions as above. Additional runs of the numerical solver used different branch cuts, none of which affected our numerical solutions. Further checks were made for λ purely real and purely imaginary to ensure no solutions there were missed. Most of our solutions correspond to the modes found by CRT. We also find a new mode barotropic mode that is analogous to a trivial solution to the eigenvalue problem in the rigid lid non-hydrostatic problem.

Completeness. Even with the inability to produce a initial value problem, a natural question to ask is if the modes we produce from (1.14) are complete, and that no additional modes our

missed in our analysis. The rigid lid modes are also known to be a complete set of solutions. And while CRT was able to prove that the hydrostatic leaky rigid lid modes were also complete, we are not able to do so here. It is not possible to use the completeness of the modes in CRT to prove completeness here by some argument of continuously transforming one problem to the other, since relaxing hydrostatic balance is a singular perturbation to the problem. In spite of this, because the modes in CRT are complete, and the additional nonhydrostatic motion can be accounted for in a novel barotropic mode in addition to modifications to the modes found by CRT, we have reason to expect that the solutions enumerated below are a complete set of solutions.

1.4. Features of the modes

The solutions of (1.14) constitute a discrete set of eigenfunctions and complex-valued eigenvalues, with decay rates and oscillation frequency given by the real and imaginary parts of $\lambda = \mu + i\omega$, as well as their complex conjugate. As a second order problem in z for all k, λ, we know that the solution space will have multiplicity of at most two. The rigid lid boundary condition then reduces the multiplicity to at most one, with the upper boundary condition serving as arbiter of λ being an eigenvalue or not.

Most of the solutions are the family of baroclinic modes, denoted by their eigenvalue λ_m for integers $m \geq 1$, which exhibits both decay and oscillation. There is also a barotropic mode with a purely imaginary eigenvalue ω_0 and a stratospheric-CRT mode with a purely real eigenvalue $\mu_- < 0$. The indexing of the barotropic and baroclinic modes reflects the vertical structure of u when decomposed as a Fourier series. The stratospheric-CRT mode generalizes the $n = 0$ mode discussed in CRT Section 4 Part d, but is notated separately due to its unique structure, with the $-$ subscript used to reflect its real decay rate. All of these solutions are parameterized using real k, since the horizontal extent of the domain is close to unbounded relative the length scale.

Beyond these caveats listed in part (a), the value of N_2 does not affect the qualitative interpretation of this section. As such, we restrict our attention to the case $N_2 = 2$ unless otherwise stated.

1.4.1. The rigid lid limit. To understand the characteristics of the leaky rigid lid, we begin with what is known about the rigid lid in the nonhydrostatic case. When $1/N_2 \to 0$, as assumed in the rigid lid case, which amounts to setting the right hand side of (1.14) to 0. The solution to

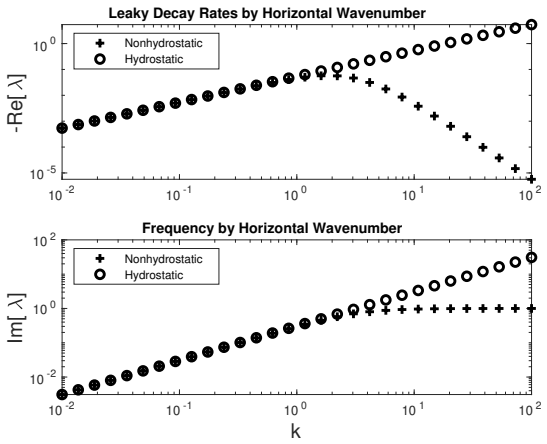

FIGURE 1.1. Comparison of the decay rates (top) and frequencies (bottom) of the first baroclinic mode for hydrostatic and non-hydrostatic atmospheres over a range of horizontal wavenumbers, $N_2 = 2$. The eigenmodes do not decay in a rigid lid atmosphere, and the choice of boundary condition does not impact the frequency structure. In the limit of small horizontal wavenumbers, the frequency of the non-hydrostatic solutions matches that of the hydrostatic solutions, as is evidenced from the overlap in the frequency plots. The frequency and decay rates of the non-hydrostatic theory deviate substantially from those of the hydrostatic theory at high horizontal wavenumber, as the frequency and decay rate of the nonhydrostatic baroclinic modes approach the barotropic mode as $k \to \infty$.

this eigenvalue problem is equivalent to (1.9) for $m \geq 0$. Relaxing hydrostatic balance introduces the k^2 term in the denominator, which has several consequences.

The first is that $m = 0$ now has a valid solution for all k. The reason no $m = 0$ mode is observed in the rigid lid is due to the boundary condition. Our new boundary condition permits such a solution, which is discussed in Part (c) of this section. When the rigid lid primitive equations are solved using Fourier series in the vertical direction, $m = 0$ denotes the barotropic terms, and we stick to this convention.

Additionally, the frequency of the $m = 0$ mode serves as a limiting frequency of the baroclinic modes as $|k| \to \infty$. As such the baroclinic modes are now dispersive, in contrast to the hydrostatic case (see Figure 1.1). In our scaling, this frequency is N_1/δ, where N_1 is the tropospheric B-V frequency. The novel feature of all of these is that this frequency is not only the short-wave limit to the frequency terms of the leaky rigid modes, it also serves as a limit for the decay rates, which is shown best in Figure 1.1.

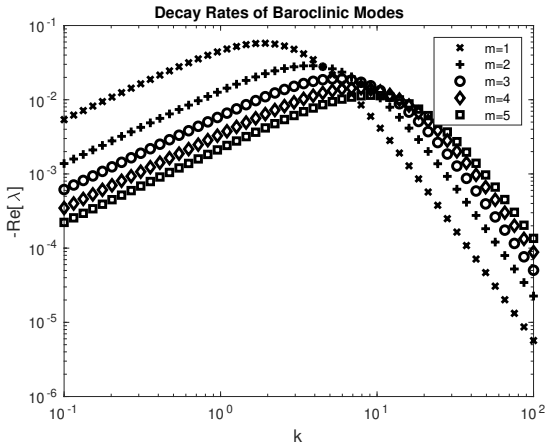

FIGURE 1.2. Decay rates for the various baroclinic modes as a function of horizontal wavenumber, using $N_2 = 2$. We observe that for each mode there is a transition from a k^1 power law in the hydrostatic limit to one of k^{-3} in the non-hydrostatic regime. Although the maximum decay rate, and the zonal wavenumber at which that maximum is achieved depend on the vertical wavenumber, the low and high wavenumber power law behavior of the decay rate as a function of horizontal wavenumber is independent of vertical wavenumber. Below we show how the decay rates for different vertical wavenumbers can be collapsed onto one function.

1.4.2. The baroclinic modes. Relaxing the rigid lid and hydrostatic assumptions for gravity waves primarily characterize the behavior of the frequency and decay rates of the baroclinic modes as a function of wavenumber.

The behavior of the frequency of the baroclinic modes, ω_m, is primarily due to whether or not the atmosphere is hydrostatic. For the hydrostatic case, the frequency of each mode is independent of the boundary condition, seen in CRT, ER and [**Lin and Emanuel, 2022**]. In the non-hydrostatic case, the boundary condition does affect the frequency, but only weakly. The effect is so insignificant that the rigid lid frequency was reliably used as an initial guess in the root-finding algorithm to find all of the λ_m. Consequently, the phase and group velocity are essentially unchanged by the boundary condition. These quantities were computed in the longwave for the leaky nonhydrostatic problem, as shown in Table 1.1, and we see general agreement with rigid lid computations and CRT.

However, the decay rates of the baroclinic modes, μ_m, are more complicated than the frequencies. When the rigid lid boundary condition is relaxed, it changes the structure of the problem in such a way that λ is no longer strictly imaginary, but its real component is non-positive, allowing for decaying modes. This was a major result of CRT, who found that for the hydrostatic leaky lid

TABLE 1.1. Properties of the baroclinic modes, by their index, with $N_2 = 2$. First row: Maximal decay rates seen in Figure 1.2. Second row: the horizontal wavenumber which corresponds to the maximum in the first row, which is in units relative to $\tilde{H}^{-1}$. Third row: Decay rates at the length scales used by CRT, and showing approximate agreement with (20) therein. Fourth row: Horizontal phase velocity in the $k \to 0$ limit, as seen in the frequency plot of Figure 1.1, which is in agreement with CRT.

Baroclinic Mode	$m = 1$	$m = 2$	$m = 3$	$m = 4$
Max Decay Time (hr)	0.48	0.97	1.45	1.96
Wavenumber of Max	1.74	3.56	5.74	7.28
CRT Decay Time (days)	1.5	5.1	11.1	19.5
Phase Velocity (m s^{-1})	49.4	25.3	17.0	12.7

atmosphere, the relation between decay rate and horizontal wavenumber was linear, $\mu_m \propto -|k|/m^2$, much like the frequency of the same modes. The nonhydrostatic problem agrees with the hydrostatic in the longwave limit, see Table 1.1 and Figure 1.1 for a comparison. Again however, the eigenvalue of the barotropic mode serves as a limit for the eigenvalue of the baroclinic modes. Since the barotropic mode is purely oscillatory, what is thus observed is a non-monotonic relation between the decay rate and the horizontal wavenumber (Figure 1.1). We find that the maximal decay rates for the gravest baroclinic modes are on time scales appropriate for thunderstorms [**Rudlosky and Fuelberg, 2013**], suggesting that this may be a mechanism contributing to their dissipation. Amidst this, there is a similarity structure that is discussed in Part (e) of this section that helps characterize this behavior.

The complex nature of λ also has consequences on the vertical structure of the modes (Figure 1.3). When the functions are scaled such that the real component vanishes at the tropopause, the real and imaginary components of the eigenfunction can be understood as the rigid and leaky components respectively. The rigid component approximates the structure of the corresponding rigid lid mode. The leaky component on the other hand oscillates and grows with until it reaches the tropopause. The rigid component has a notably larger amplitude than the leaky component, even when compared to the ratios of the hydrostatic case, which also agrees with Figure 5 of [**Lin and Emanuel, 2022**].

1.4.3. The barotropic mode. The barotropic mode corresponds to the $m = 0$ case of the nonhydrostatic rigid lid problem, having frequency $\omega_0 = 1$ from our chosen values of N_1, δ. If we

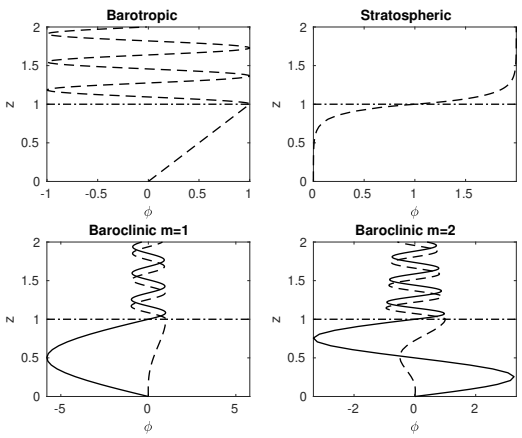

FIGURE 1.3. Various modes produced by the nonhydrostatic leaky lid equations, $N_2 = 2$ and $k = 10$. The solid line indicates the rigid component of each mode, and the dashed line indicates the leaky component. The mode is scaled such that the leaky component takes a unit value at the tropopause ($z = 1$).

consider solutions of the form $\phi(z)e^{ikx+it}$, the tropospheric equations reduce to

$$\phi_{zz} = 0, \quad 0 < z < 1,$$

$$\phi = 0, \quad z = 0. \tag{1.15}$$

The vertical structure is a linear profile, which would has a trivial solution when paired with rigid lid boundary conditions. In addition to the aforementioned reasons for calling it barotropic, a linear profile of ϕ corresponds to a uniform vertical structure of horizontal winds. The value λ_0 is the solution resulting from the singular perturbation of relaxing hydrostatic balance, however the existence of a non-trivial mode also requires appropriate boundary conditions, which the rigid lid does not satisfy.

1.4.4. The stratospheric-CRT mode. This mode is notable in that λ is real and negative, and consequently does not have a rigid lid counterpart. This was a novel result in CRT, who label it $n = 0$. Due to the aforementioned indexing conflict, we instead refer it as the stratospheric-CRT mode, since it is mostly nonzero near the tropopause as $k \to \infty$. It shares many of the same properties such as the nonoscillatory vertical structure, and vanishing as $N_2 \to 1$.

The decay rate of this mode is significantly stronger than that of the corresponding set of generic modes, which is described by CRT as a "fast adjustment". CRT is able to compute this analytically by $\mu_- = -|k| \tanh^{-1}(1/N_2)$, but to find it numerically, we begin with the empirical

estimate $\mu_- \sim -e^{|k|}\tanh^{-1}(1/N_2)$. This indicates that as we investigate smaller scales, it decays significantly faster than any other process, especially with the baroclinic decay rates becoming weakened by loss of hydrostatic balance and the introduction of the barotropic mode. Since it is so fast, it imposes a constraint on the time step for a numerical simulation of gravity waves in a similar fashion as acoustic waves. However unlike acoustic waves, it is unknown if they carry significant amounts of kinetic energy to dissipate. This and our statements regarding the non-monotonic decay rates of the baroclinic modes do not conflict with the decay rates computed by CRT since they agree in the limit $k \to 0$ as expected.

1.4.5. Similar decay characterization in the baroclinic modes. However, when we compare one baroclinic mode to the other, we have the option to instead define the characteristic height and length in terms of the wave numbers. Doing so implies the existence of a similarity in the decay rates across the baroclinic modes. As such, we find the decay rates follow a profile

$$\mu(k, m; N_2) = \frac{-1}{\pi m} f\left(\frac{|k|}{\pi m}; N_2\right). \tag{1.16}$$

The example of function $f(\theta; N_2 = 2)$ is plotted in Figure 1.4, in terms of the angle of the wavenumber vector from the horizontal (or the angle of the wave front from the vertical), $\theta = \cot^{-1}(|k|/(\pi m))$. Testing for various N_2 values from 1 to 10, we find that the qualitative behavior of f does not vary significantly, and that the similarity remains robust up to the vanishing lid limit $N_2 \to 1$. The m^{-1} leading factor corresponds to the fact that waves of smaller vertical length have to travel proportionally farther before encountering the tropopause. We note agreement with the approximation $\mu \sim -|k|/N_2(\pi m)^2$ used in (15) of CRT for the hydrostatic decay rates in the long wave limit.

A consequence of this scaling is that the time dependence of a wave can be characterized primarily by its angle from the horizontal and the $1/(\pi m)$ factor. For small values of $|k|/(\pi m)$, the waves travel upward, radiating through the tropopause, and decaying like the hydrostatic modes computed by CRT. For large values of $|k|/(\pi m)$, the waves travel nearly horizontally, and behave much like the barotropic mode in being in that they decay slowly in time and have a velocity field which is nearly horizontal in time. Based on the similarity profile shown in Figure 1.4, for a fixed vertical wavenumber, the decay is maximal a approximately a 60° angle from the horizontal.

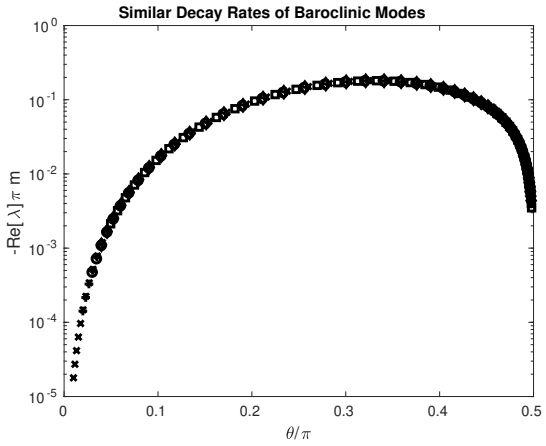

FIGURE 1.4. Similar solutions for the decay rates across several baroclinic modes, for $m = 1...5$. This examines the structure in terms of the angle of the wavenumber vector from the horizontal, with the maximum decay occurring at about 60°. This matches the asymptotic power laws in Figure 1.2, keeping in mind that the angle close to $\pi/2$ corresponds with the longwave limit.

This analysis provides a geometric framework for tropospheric wave dissipation in terms of hydrostatic adjustment on air columns across the tropopause. When the wave travels close to vertically, the perturbation mostly remains in the same air column, and so most of the necessary energy to restore hydrostatic balance remains within the column. As such energy dissipates slowly, and a vertically traveling wave ($k = 0$) would in theory never dissipate. However, a wave traveling at an angle arrives at the tropopause away from its original air column, and energy is spent trying to reestablish hydrostatic balance to both columns. This is also a feature of the low wavenumber regime of CRT.

However, as the wavefront travels closer to horizontally, energy crosses the tropopause more slowly, so the dissipation slows down. It is important to note that this does not take into account other dissipative mechanisms such as the effects of surface friction, which [**Lin and Emanuel, 2022**] determine is additive with stratospheric damping, with the note that they assume hydrostatic balance on the equatorial scale.

1.5. Approximate decay operator

While the similarity profile does not have a closed form, we can use the limiting asymptotics in $|k|$ to get an estimate of μ. In the longwave limit, it grows as $O(|k|)$ like the hydrostatic problem. In the high wavenumber limit, the decay rate shrinks like $O(|k|^{-3})$, as observed in Figure 1.2. Based

on these asymptotics and the similarity assumption, we can fit the decary rate to the curve

$$\mu = \frac{-b|k|\pi^2 m^2}{(\pi^2 m^2 + a^2 k^2)^2} \tag{1.17}$$

where a, b are coefficients that control the asymptotics in the large and small $|k|$ regimes respectively. An empirical fit determines that $a^2 = 0.96, b = 0.54$ estimates λ for $N_2 = 2$, with at most 2% relative error across all k.

This analytic form also allows us to express the damping in the rigid lid approximation not as a boundary condition, but as an operator on the interior attached to the time derivatives. To do so, we invert the Fourier transform of (1.17), and arrive at the linear operator,

$$D = b\partial_{zz} H[\partial_x](-\Delta_a)^{-2}, \tag{1.18}$$

where H is the Hilbert transform, and the inverse of the anisotropic Laplacian is $\Delta_a = \partial_{zz} + a^2\partial_{xx}$. Since our measured a^2 is close to 1, the possibility emerges of using the isotropic Laplacian Δ_1, at the expense of an increase in maximum relative error to 6%.

We compute this operator in order to contrast it with other damping operators, such as linear damping and (hyper-)viscosity. As a damping term, we include it in the original equations as follows,

$$\begin{aligned} \rho_0 u_t + p_x &= D\rho_0 u, \\ \rho_0 w_t + p_z + g\rho &= D\rho_0 w, \\ \rho_t + \rho_{0z} w &= D\rho, \text{ and} \\ u_x + w_z &= 0. \end{aligned} \tag{1.19}$$

We believe that this approximation might provide a model for the gravity wave decay of the baroclinic modes in rigid lid simulations using Fourier spectral methods. The damping operator in Equation (1.17) could be used while computing the operators in Fourier space with rigid lid boundary conditions. Since D is a differential operator, formal considerations of its use would require additional analysis of the equations, as would be required if one were to use a tradional Stokes, or hyper-diffusive damping term. Furthermore, given that an initial value problem cannot

be fully posed with our boundary condition, this may be the closest way to approximate gravity wave drag.

1.6. Conclusions

The leaky rigid lid boundary condition was introduced by [**Chumakova et al., 2013**] to resolve the question of whether tropospheric dynamics could be usefully modelled with a vertically finite atmosphere. They concluded that it can be. We extend this framework by considering what happens in a two-layer, infinite, nonhydrostatic atmosphere, to better understand the behavior of these waves at small horizontal scales. The vertical structure of these waves suggest that the waves do exist in an infinite atmosphere, but they are trapped near the tropopause, thereby yielding a discrete spectrum of modes. The question of how to define a boundary condition to solve the problem exclusively in the troposphere remains.

In addition to the discrete family of baroclinic modes common to the rigid lid problem, plus the stratospheric-CRT mode, relaxing the hydrostatic approximation introduces a new barotropic mode that is compatible with the jump conditions at the tropopause. The frequency of this mode serves as a limit to the decay rate and frequency of the baroclinic modes in the limit of large horizontal wavenumber. As a result, the decay becomes a nonlinear function in $|k|$, the horizontal wavenumber differing from the hydrostatic atmosphere.

The behavior of the barcolinic modes is primarily characterized by the angle of elevation of the wave front. That the decay rate is a function of the angle of the wavefront could be useful in providing a geometric explanation to various observed phenomena. We found that the maximum decay rates corresponded to a front moving at an angle of about 60° from the horizontal.

Using the limiting asymptotics of the decay rate curve and the angular properties, an estimate for the decay rates was derived in general agreement with the actual decay. A linear operator was then found that can produce the decay for the baroclinic modes, even in a rigid lid system. The non-hydrostatic leaky rigid lid theory provides a model to study the dynamics of gravity waves while incorporating the effects of stratospheric wave radiation.

CHAPTER 2

Unidirectional Dispersive Waves

2.1. Introduction

The simplest way to account for the behavior of a family of waves is to consider its linear dispersion relation $F(\omega, k) = 0$ for wavenumber k and frequency ω, often expressed as a set of functions $\omega_i(k)$. A dispersive wave is a wave with non-constant group velocity $\frac{d\omega}{dk}$. A unidirectional wave is a one-dimensional wave whose phase velocity $\frac{\omega}{k}$ is the same sign across all wave numbers. Among these unidirectional waves, we consider the subset where $\lim_{k\to 0} \omega(k)\text{sgn}(k) = \omega_0 \neq 0$, which we call a frequency jump. In this paper we study two examples of nonlinear interactions of dispersive, unidirectional waves with a frequency jump via multiscale asymptotics in the low wavenumber limit.

A number of previous works apply similar asymptotic analyses on similar but distinct problems. J.P. Boyd used this to describe the nonlinear behavior of equatorial waves, starting with the dispersionless, unidirectional Kelvin wave [**Boyd, 1980b**], before moving on to the weakly dispersive unidirectional equatorial Rossby waves [**Boyd, 1980a**], which lack the strong dispersion studied herein, and the frequency jump. Boyd then completed his study of the equatorial waves by considering the strongly dispersive waves with potential for a frequency jump [**Boyd, 1983a**], but distinguished the waves by the sign of their frequencies, and not their phase velocities. Further description of Boyd's work begins section 3. A similar approach is used in studying the Sine-Gordon equation as seen in [**Rosales, 2003**]. Finally, [**Biello and Hunter, 2010**] studies the behavior of a unidirectional wave with frequency jump, lacking dispersion. One interesting property of the equatorial waves is that there is an asymmetry between eastward and westward waves, and so distinguishing the two may be important. As such, we apply the techniques of [**Biello and Hunter, 2010**] to the strongly dispersive waves of [**Boyd, 1983a**], in particular, we examine the results on the Yanai waves. To understand these techniques in a simpler light, we also apply this analysis to the Sine-Gordon equation.

Following in the wake of these previous analyses, we use a weakly nonlinear expansion, which at first order linearizes the system, resulting in a linear dispersion relation in the low wavenumber regime. One of the consequences of operating in the low wavenumber regime is that spatial derivatives are of higher order in the expansion. At the higher orders, nonlinear terms act as a signed sum of frequencies and wavenumbers of the various waves, which resonate if this signed sum simultaneously matches the linear dispersion relation in both frequency and wavenumber. To resolve any resonance, a long time scale is introduced which produces a long time solvability condition for the wave packet. To properly handle the unidirectional aspect, a Hilbert transform in space is used to distinguish the waves going in the different directions.

We consider two examples in this paper. First, we look at the Sine-Gordon equation from particle physics, to demonstrate the essence of the method. Second, we consider the Yanai wave from equatorial dynamics, whose longwave components are a prominent feature in the observational record despite an observed asymmetry in the zonal phase velocity. In both cases, we find the asymptotics are dictated by an equation that is essentially the Nonlinear Schrodinger equation.

2.2. Sine-Gordon

One example of a dispersive nonlinear equation is the Sine-Gordon equation, whose weakly nonlinear expansion is well understood to characterize breather solutions [**Rosales, 2003**]. To focus upon the unidirectional problem, we consider the simplest nonlinearity from the Sine-Gordon equation,

$$u_{TT} - u_{XX} + \sin(u) = 0. \tag{2.1}$$

We decouple the time scales to $t = T, \tau = \frac{1}{2}\epsilon^2 T$, which yields the derivative $\partial_{TT} = \partial_{tt} + \epsilon^2 \partial_{t\tau} + \frac{1}{4}\epsilon^4 \partial_{\tau\tau}$. We also work in the single long variable $x = \epsilon X$. Like the other problems previously considered, we use the weakly nonlinear expansion $u = \epsilon u_1 + \epsilon^2 u_2 + \epsilon^3 u_3 + O(\epsilon^4)$. At $O(\epsilon)$ through $O(\epsilon^3)$, we have

$$u_{1tt} + u_1 = 0 \tag{2.2a}$$

$$u_{3tt} + u_3 = -u_{1t\tau} + u_{1xx} + \frac{1}{6}u_1^3. \tag{2.2b}$$

The $O(\epsilon)$ equation is often decomposed as $(\partial_t + i)(\partial_t - i)u_1 = 0$, which has a solution of the form $u_1 = f(x,\tau)e^{-it} + g(x,\tau)e^{+it}$, which are the positive and negative frequency solutions respectively. However we could also factor this by using the Hilbert transform in spatial variable. The Hilbert Transform $\mathcal{H} : L^2(\mathbb{R}) \to L^2(\mathbb{R})$ is defined here by

$$\mathcal{H}[e^{ikx}] = -i\text{sgn}(k)e^{ikx}. \tag{2.3}$$

Note that it satisfies $\mathcal{H} \circ \mathcal{H} = -Id$ (the identity operator) on $L^2(\mathbb{R})$. Any automorphism which satisfies that identity can be used to build a linear complex structure, enabling the use of many of the properties of complex variables. We use algebraic closure to refactor the equation as $(\partial_{tt} + 1)u_1 = (\partial_t + \mathcal{H})(\partial_t - \mathcal{H})u_1 = (\partial_t - \mathcal{H})(\partial_t + \mathcal{H})u_1 = 0$, which we can split to the linear Hilbert equation. The generic solution to this problem is $u = e^{tH}f(x,\tau) + e^{-tH}g(x,\tau)$, now denoting the terms with positive and negative phase velocity respectively. The time evolution operator can be expanded as

$$e^{tH}f = (\cos(t) + \sin(t)\mathcal{H})f(x,\tau) \tag{2.4}$$

via Euler's identity applied to the Hilbert transform. To investigate the effect of unidirectionality we consider $g(x,\tau) = 0$, or $u_t = \mathcal{H}[u]$. Euler's identity also gives a way to account for phase shifts in the wave without the explicit use of complex numbers, which significantly simplifies the analysis. In effect this changes the system into

$$(\partial_t - \mathcal{H})(2\mathcal{H}[u_1]) = 0 \tag{2.5a}$$

$$(\partial_t - \mathcal{H})(2\mathcal{H}[u_3]) = -\mathcal{H}[u_1]_\tau + u_{1xx} + \frac{1}{6}u_1^3. \tag{2.5b}$$

To be asymptotically consistent, the right hand side must satisfy the Fredholm alternative for this problem, which here states the equation

$$u_t - \mathcal{H}[u] = e^{\alpha t\mathcal{H}}B(x) \tag{2.6}$$

has the particular solution $e^{\alpha t\mathcal{H}}A$, where $A = \frac{\mathcal{H}[B]}{1-\alpha}$. This produces an acceptable solution for $\alpha \neq 1$, and requires the condition $B = 0$ if $\alpha = 1$ (Proposition 4.1, [**Biello and Hunter, 2010**]). This condition becomes our solvability requirement at $O(\epsilon^3)$ in both cases. At $O(\epsilon^2)$ we note that the homogeneous solution can be arbitrarily absorbed into the $O(\epsilon)$ solution. No particular solution is

needed at this order, but would be necessary if we had a quadratic nonlinearity, to be seen in the atmospheric example, but eschewed here for clarity. At $O(\epsilon^3)$ we expand the nonlinear contribution to find its resonant terms

$$u_1^3 = \frac{3}{4}(f^2 + (\mathcal{H}f)^2)e^{t\mathcal{H}}f + e^{3t\mathcal{H}}\left(\frac{1}{3}f^3 - f\mathcal{H}[f]^2\right) \tag{2.7}$$

and apply the solvability condition from (2.6) to the resonant terms of (2.5c) to obtain the long time evolution equation

$$-\mathcal{H}[f]_\tau + f_{xx} + \frac{1}{8}(f^2 + \mathcal{H}[f]^2)f = 0. \tag{2.8}$$

While this appears to be novel, this is similar to the Nonlinear Schrodinger (NLS) equation,

$$if_\tau + f_{xx} + \frac{1}{8}|f|^2 f = 0. \tag{2.9}$$

Both of these equations operate over a linear complex structure, but with different automorphisms, $\mathcal{H}$ and i respectively. These automorphisms both act on the f_τ terms directly, and the $f^2 + \mathcal{H}[f^2]$ captures the modulus of the function when presented as $f + i\mathcal{H}f$, which is analogous to $|f|^2$.

One feature that significantly streamlines this problem is the cubic nonlinearity, where the interactions of the wave with itself can produce a response at the same frequency (i.e. $\pm 1 \pm 1 \pm 1 = \pm 1, \pm 3$). By contrast, the Burgers-Hilbert equation and the equatorial waves have a quadratic nonlinearity, which does not produce a response at the same frequency (i.e. $\pm 1 \pm 1 = 0, \pm 2$), so resonance may arise on if the quadratic response interacts with the linear wave (e.g. $u_1 u_2$).

2.3. Equatorial Waves

Convectively coupled equatorial waves play an important role in the control of tropical precipitation. The horizontal properties and dispersion of these waves are first unified in [**Matsuno, 1966**] from the linear theory of the equatorial shallow water equations. These solutions describe a family of discrete waves with a meridional index m, named the Kelvin ($m = -1$), equatorial Rossby ($m \geq 1$), mixed Rossby-gravity (MRG)($m = 0$), and east/west inertio-gravity (EIG/WIG) ($m \geq 0/m \geq 1$) waves in a unified manner over the equatorial β plane.A review of the importance of these waves can be found in [**Kiladis et al., 2009**].

One major development of the theory was to incorporate the effects of nonlinear advection of the shallow water equations via multiscale asymptotics. This was done by Boyd in the early 1980's using the weakly nonlinear expansion. One of the main distinctions that is made for the asymptotics is the dispersion of the linear wave, which determine both the long time scale in terms of ϵ(the amplitude of the linear wave) and the equation that describes it. Boyd's study of equatorial waves using these techniques starts in [**Boyd, 1980b**], which describes the nonlinear Kelvin wave, which operates on a time scale $\tau = \epsilon t$. The solvability condition is the inviscid Burgers' equation where the advection dominates dispersion (since there is none). For long Rossby waves, [**Boyd, 1980a**] computes that the solvability condition is the (modified) Korteweg-deVries ((M)KdV) equation for $\tau = \epsilon^{3/2}(\epsilon^3)$ for odd (even) meridional index, which the weak dispersion of the wave balances the advection. In [**Boyd, 1983a**], all other waves have strong dispersion that dominates the advection, and are described using a NLS equation on a time scale $\tau = \epsilon^2$.

Boyd's program saw a few additional developments over the years. Most of the strongly dispersive waves are described using the NLS model from [**Boyd, 1983a**] that capture four wave resonances, but there are some three wave resonances in the long wave and second harmonic interactions that are fleshed out in [**Boyd, 1983b**, **Boyd, 1983c**]. In [**Majda et al., 1999**], the long Kelvin waves are coupled to other large scale equatorial waves via topographic resonance in an effort to mitigate the breaking inherent to the inviscid Burgers' equation. In [**Majda and Biello, 2003**, **Biello and Majda, 2004**], a multilayer model is used to investigate the resonant interaction between the baroclinic and barotropic Rossby waves, which has significant implications on the study of teleconnections between the tropics and midlatitudes.

This theory assumed a wave packet centered about some fixed zonal wavenumber $k = k_0$. The group velocity $\frac{d\omega}{dk}$, is computed using the dispersion relation of the wave, which has nondimensional form

$$\omega^2 - k^2 - \frac{k}{\omega} = 2m + 1 \tag{2.10}$$

Since the dispersion is characterized a relation and not a function, there is the possibility of multiple frequencies operating at the same zonal and meridional numbers. For most k this is not an inherent problem, since the dispersion relations for the Matsuno modes are discrete, disconnected branches where the frequency and phase speed change continuously. The exception to this at $k = 0$, where

the phase speed diverges for many of the waves. There are two possibilities to describe the wave over the positive and negative wavenumbers: to keep the sign of the frequency the same, or to change the sign of the frequency, but keep the phase velocity in the same direction. This choice of description is examined in Figure 2.1, where we can either consider the waves as distinguished by their frequency or phase velocity. In his paper, Boyd implicitly makes the choice to keep the frequency continuous. In contrast, we make the latter choice, which is the distinction that is generally used to distinguish the waves [**Kiladis et al., 2009**]. This will allow us to consider one wave, for example the EIG0 wave, without having to consider its counterpart, in this case the MRG wave. Furthermore, in making the latter choice, the waves will satisfy the condition $\omega(-k) = -\omega(k)$, which ensures they will be real-valued.

Here we investigate the consequences of choosing unidirectional waves, specifically for meridional index 0, corresponding to the MRG and EIG0 waves, collectively called the Yanai wave. This wave has been observed to have strong OLR (outgoing longwave radiation) signal in the low zonal wavenumber limit (see Figure 2.2). Our analysis was done in an effort to determine if the long-time evolution equation would produce a soliton that woud cause this signal to appear. A multiscale analysis of another unidirectional wave in the same limit was done previously [**Biello and Hunter, 2010**] on the Burgers'-Hilbert equation, which capture the solvability condition as a cubic nonlinear equation. One major distinction to be made is that the linear Burgers'-Hilbert equation is nondispersive, but the Yanai wave is.

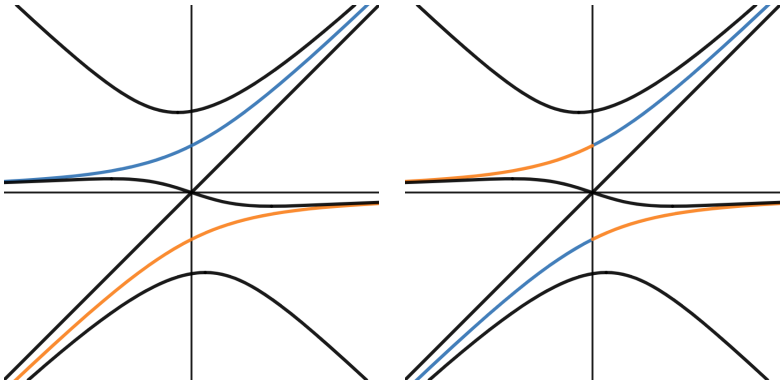

FIGURE 2.1. The dispersion relations of the simplest equatorial waves (meridional index $m \leq 1$), with the $m = 0$ waves distinguished in two different ways. (a) has them split by sign of the frequency, which will have solutions of the form $e^{\pm i\omega(k)t}$, whereas (b) has them split by sign phase velocity, which will have solutions of the form $e^{\pm i \mathrm{sgn} k \omega(k)t}$. Colored in (b) are the MRG (orange) and the EIG $m = 0$ (blue) waves.

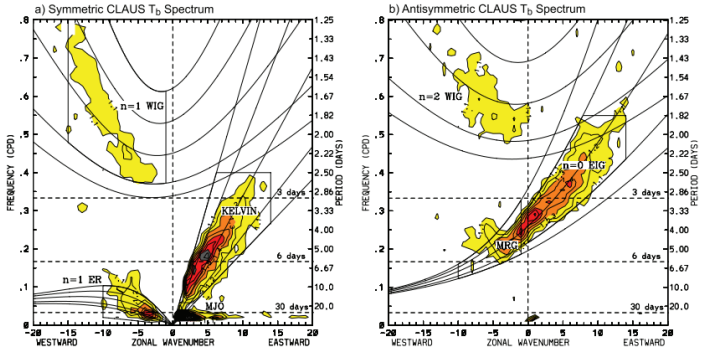

FIGURE 2.2. OLR observations of he Matsuno modes plus the Madden Julian Oscillation. We observe in b), a strong signal at zonal wavenumber 0 in the Yanai frequency band. It is this signal that we attempt to understand via this analysis. (Used with permission from [**Kiladis et al., 2009**]).

2.3.1. Derivation of the Long Time Behavior. Our derivation begins with the nonlinear equatorial shallow water equations

$$u_t - yv + p_x = -uu_x - vu_y, \tag{2.11a}$$

$$v_t + yu + p_y = -uv_x - vv_y, \tag{2.11b}$$

$$p_t + u_x + v_y = -(up)_x - (vp)_y, \tag{2.11c}$$

Where x, y are the zonal and meridional coordinate and u, v are their respective velocities. p is scaled to the depth of the fluid layer H. Velocities are scaled to the dry gravity wave speed $c = \sqrt{gH}$, where g gravitational constant. The horizontal lengths are scaled by the equatorial deformation radius $\sqrt{c/\beta}$, where β is the meridional gradient of the Coriolis force at the equator. This generates the time scale $\sqrt{c\beta}$.

The high-frequency equatorial long waves all have a nonzero group velocity, which is resolved by working in a coordinate moving in the zonal direction, which has the following defining properties

$$\theta = x - c_g t, \quad \partial_x = \partial_\theta, \quad \partial_t = \partial_t - c_g \partial_\theta.$$

For our analysis of the MRG and EIG0 waves, we cancel out the longwave group velocity by using $c_g = \frac{d\omega}{dk}|_{k=0} = \frac{1}{2}$, which is computed via (2.10). As stated from the outset, we consider the analysis for weakly nonlinear waves, i.e. solutions will take the form $\psi = (u^\epsilon, v^\epsilon, p^\epsilon)$ where

$$f^\epsilon = \epsilon f_1 + \epsilon^2 f_2 + \epsilon^3 f_3 + O(\epsilon^4)$$

We work in a strictly long wave expansion $\partial_\theta = O(\epsilon)$, which differs from the long wave expansions of the low frequency equatorial waves where ∂_t and $|v|$ are also $O(\epsilon)$, though this comes into play when we analyze the low frequency responses to the nonlinear interactions. We also define $\tau = \epsilon^2 t$ as the long time scale, which is the appropriate scale for the strongly dispersive waves found in [**Boyd, 1983a**].

2.3.2. Linear Response. We start again our expansion at $O(\epsilon)$, denoted $L\psi_1 = 0$.

$$u_{1t} - y v_1 = 0 \tag{2.12a}$$

$$v_{1t} + y u_1 + p_{1y} = 0 \tag{2.12b}$$

$$p_{1t} + v_{1y} = 0 \tag{2.12c}$$

We use the Yanai wave solution, which takes the form $u_1 = p_1 = Q(\theta, t, \tau) y G(y)$, $v_1 = V(\theta, t, \tau) G(y)$, where $G(y) = e^{-y^2/2}$, to get the reduced system

$$Q_t - V = 0$$

$$V_t + Q = 0,$$

which may also be expressed in the single equation $Q_{tt} + 1 = 0$. Implicitly in [**Boyd, 1983a**] this equation is factored as $(\partial_t + i)(\partial_t - i)Q = 0$ to produce solutions of e^{it}, e^{-it}, which splits the waves into positive and negative frequencies. However, we decompose by the sign of phase velocity via a Hilbert transform in θ, as previously done. This produces two solutions corresponding to the MRG and EIG0, denoted $M(\theta, t, \tau)$ and $E(\theta, t, \tau)$ respectively. The full solution to this problem is

$$\begin{pmatrix} u_1 \\ v_1 \\ p_1 \end{pmatrix} = \begin{pmatrix} \tilde{u} \\ 0 \\ \tilde{p} \end{pmatrix} + \begin{pmatrix} (E+M)yG(y) \\ (\mathcal{H}[E] - \mathcal{H}[M])G(y) \\ (E+M)yG(y) \end{pmatrix} \tag{2.13}$$

Where $y\tilde{u} + \tilde{p}_y = 0$ denotes the stationary geostrophic solution, which we neglect since that is not part of the Yanai wave. When [**Boyd, 1983a**] derived the NLS equation, he examined both waves operating at the same frequency. We now can isolate either the MRG or EIG0 waves and investigate their long time asymptotics independently. To avoid the complications of handling the Hilbert transform on all positive and negative zonal wavenumbers, we only analyze what happens for positive zonal wavenumbers and then solve for the negative zonal wavenumbers via symmetry. For the MRG wave, we define

$$M(\theta, t, \tau) = F(\theta, \tau)e^{it} + F^*(\theta, \tau)e^{-it} \tag{2.14}$$

where $F(\theta, \tau) = \int_0^\infty \hat{F}(k, \tau)e^{ik\theta}dk$. We compute

$$-\mathcal{H}[M] = iF(\theta, \tau)e^{it} - iF^*(\theta, \tau)e^{-it}. \tag{2.15}$$

For the EIG0 wave, we in a similar manner define

$$E(\theta, t, \tau) = D(\theta, \tau)e^{-it} + D^*(\theta, \tau)e^{it}, \tag{2.16}$$

$$\mathcal{H}[E] = -iD(\theta, \tau)e^{-it} + iD^*(\theta, \tau)e^{it}. \tag{2.17}$$

where $D(\theta, \tau) = \int_0^\infty \hat{D}(k, \tau)e^{ik\theta}dk$. We consider the longwave limit of the MRG wave alone, analysis for the EIG0 wave can be achieved at any stage by the substitution $F \to D^*$

2.3.3. Non-Linear Interactions. At $O(\epsilon^2)$,

$$L\psi_2 = \begin{bmatrix} -v_1 u_{1y} + \frac{1}{2}u_{1\theta} - p_{1\theta} \\ -v_1 v_{1y} + \frac{1}{2}v_{1\theta} \\ -(v_1 p_1)_y + \frac{1}{2}p_{1\theta} - u_{1\theta} \end{bmatrix} \tag{2.18a}$$

There are three main classes of response: the fundamental mode at frequency 1, the stationary mode at frequency 0, and the second harmonic at frequency 2. Variables will be denoted ψ_n^k, where k indicates the frequency, and n denotes the order of ϵ^n. An important feature to note is that time derivatives at each frequency will be captured via the operator $-k\mathcal{H}$ since we consider waves of the form $e^{-kt\mathcal{H}}\psi_n^k$. The computation of the nonlinearities at second and third order marks the largest difference between this problem and the Sine-Gordon example, especially since we are here entirely concerned with quadratic nonlinearities, in contrast to the cubic nonlinearity of Sine-Gordon.

2.3.3.1. *Behavior of the Fundamental Frequency Mode.* We consider the response at second order at the fundamental frequency, which is described by the system

$$-\mathcal{H}[u_2^1] - yv_2^1 = -\frac{1}{2}\partial_\theta M(yG(y)) \tag{2.19a}$$

$$-\mathcal{H}[v_2^1] + yu_2^1 + p_{2y}^1 = -\frac{1}{2}\partial_\theta \mathcal{H}[M](G(y)) \tag{2.19b}$$

$$-\mathcal{H}[p_2^1] + v_{2y}^1 = -\frac{1}{2}\partial_\theta M(yG(y)) \tag{2.19c}$$

The solution to which is

$$u_2^1 = p_2^1 = -\partial_\theta \mathcal{H}[M](\frac{1}{2}yG(y)), \quad v_2^1 = 0 \tag{2.20}$$

in agreement with Boyd's work. We define $F^i(y)$ denote the $O(\epsilon^2)$ meridional profile of field F at frequency i (e.g. $U^1(y) = P^1(y) = \frac{1}{2}yG(y)$).

2.3.3.2. *Behavior of the Stationary Mode.* In the low frequency regime, we see the nonlinear interaction between the MRG and EIG0. Projecting the stationary terms onto the system we get,

$$-yv_2^0 = 0, \tag{2.21a}$$

$$yu_2^0 + p_{2y}^0 = F_2, \tag{2.21b}$$

$$v_{2y}^0 = 0, \tag{2.21c}$$

where F_2 is the meridional stationary forcing that disrupts geostrophic balance, and this leads to a ill-posed problem in the standard scaling. We resolve this by using the long wave scaling, which balances $\tilde{v}_3$ (denoted differently to reflect that it comes from a lower order) against the zonal derivatives of u, p and the forcing of the same equations to produce the system

$$-\frac{1}{2}u_2^0 - y\tilde{v}_3^0 + p_2^0 = A \tag{2.22a}$$

$$yu_2^0 + p_{2y}^0 = B \tag{2.22b}$$

$$-\frac{1}{2}p_2^0 + \tilde{v}_{3y}^0 + u_2^0 = C. \tag{2.22c}$$

The forcing terms are defined as follows, some of which are expressed by their zontal derivative as part of the scaling process

$$A_\theta = -u_1 u_{1\theta} - v_2^1 u_{1y} - v_1 u_{2y}^1 = -|F|_\theta^2 \left[\frac{1}{2}y^2 + \frac{1}{2}\right] G(y)^2 \tag{2.23a}$$

$$B = -v_1 v_{1y} = |F|^2[2y]G(y)^2 \tag{2.23b}$$

$$C_\theta = -(u_1 p_1)_\theta - (v_2^1 p_1)_y - (v_1 p_2^1)_y = -|F|_\theta^2 \left[y^2 + \frac{1}{2}\right] G(y)^2. \tag{2.23c}$$

This will have a solution at $O(\epsilon)$ of the form

$$\begin{pmatrix} u_2^0 \\ v_2^0 \\ p_2^0 \end{pmatrix} = (|F|^2)(\theta, \tau) \begin{pmatrix} U^0(y)G(y) \\ 0 \\ P^0(y)G(y) \end{pmatrix}. \tag{2.24}$$

To arrive at this solution, we define variables $S = u_2^0 + p_2^0, D = u_2^0 - p_2^0$. We then decompose everything in terms of Hermite functions an orthonormal basis $\{\phi_m\}$ of $L^2(\mathbb{R})$ (see Appendix A for further details). We thus can decompose $F(y) = \sum_m f_m \phi_m(y)$ via the projection $f_m = \int_{\mathbb{R}} F\phi_m dy$. This produces a single equation $\frac{1}{2}S_0 = (F_1)_0 + (F_3)_0$ and a sequence of triples

$$\begin{bmatrix} 1/2 & -\sqrt{2(m+1)} & 0 \\ \sqrt{(m+1)/2} & 0 & \sqrt{m/2} \\ 0 & -\sqrt{2m} & -3/2 \end{bmatrix} \begin{bmatrix} S_{m+1} \\ \tilde{v}_m \\ D_{m-1} \end{bmatrix} = \begin{bmatrix} A_{m+1} + C_{m+1} \\ B_m \\ A_{m-1} - C_{m-1} \end{bmatrix} \tag{2.25}$$

The full details of this method are discussed in (3.22) - (3.30) of [**Boyd, 1983a**], though the projections were done via MATLAB. The solutions to this construct u_2^0, p_2^0 via S, D.

2.3.3.3. *Behavior of the Second Harmonic.* We consider now the second harmonic response that happens at frequency ± 2. The system at frequency 2 is described ($\partial_t = -2\mathcal{H}$) by

$$-2\mathcal{H}u_2^2 - yv_2^2 = iF^2e^{2it}[y^2-1]G(y)^2 \tag{2.26a}$$

$$-2\mathcal{H}v_2^2 + yu_2^2 + p_{2y}^2 = -F^2e^{2it}[y]G(y)^2 \tag{2.26b}$$

$$-2\mathcal{H}p_2^2 + v_{2y}^2 = iF^2e^{2it}[2y^2-1]G(y)^2 \tag{2.26c}$$

We begin by applying $\mathcal{H}$ to the zonal and pressure equations, which will have everything in phase, producing a system

$$2u_2^2 - y\mathcal{H}v_2^2 = F^2e^{2it}[y^2-1]G(y)^2 \tag{2.27a}$$

$$-2\mathcal{H}v_2^2 + yu_2^2 + p_{2y}^2 = -F^2e^{2it}[y]G(y)^2 \tag{2.27b}$$

$$2p_2^2 + \mathcal{H}[v_{2y}^2] = F^2e^{2it}[2y^2-1]G(y)^2 \tag{2.27c}$$

Solutions take the form after undoing the Hilbert transform on v_2^2

$$\begin{pmatrix} u_2^2 \\ v_2^2 \\ p_2^2 \end{pmatrix} = F^2(\theta,\tau) \begin{pmatrix} U^2(y)G(y) \\ iV^2(y)G(y) \\ P^2(y)G(y) \end{pmatrix} e^{2it} + c.c. \tag{2.28}$$

Where U^2, V^2, P^2 can be solved by a similar method as the stationary response. The first equation is $2S_0 = (F_1)_0 + (F_3)_0$, and the triplet of equations are now

$$\begin{bmatrix} 2 & -\sqrt{2(m+1)} & 0 \\ \sqrt{(m+1)/2} & -2 & \sqrt{m/2} \\ 0 & -\sqrt{2m} & 2 \end{bmatrix} \begin{bmatrix} S_{m+1} \\ v_m \\ D_{m+1} \end{bmatrix} = \begin{bmatrix} A_{m+1} + C_{m+1} \\ B_m \\ A_{m-1} - C_{m-1} \end{bmatrix} \tag{2.29}$$

All of the same caveats applied in this solution method.

2.3.4. Solvability Condition. Here we see the full effects of resonance, and so we generate the solvability condition for the following

$$L\psi_3 = \begin{bmatrix} R_u \\ R_v \\ R_p \end{bmatrix} = \begin{bmatrix} -u_{1\tau} - u_1 u_{1\theta} & -v_1 u_{2y} - v_2 u_{1y} & +\frac{1}{2}u_{2\theta} - p_{2\theta} \\ -v_{1\tau} - u_1 v_{1\theta} & -(v_1 v_2)_y & +\frac{1}{2}v_{2\theta} \\ -p_{1\tau} - (u_1 p_1)_\theta & -(v_1 p_2)_y - (v_2 p_1)_y & +\frac{1}{2}p_{2\theta} - u_{2\theta} \end{bmatrix} \tag{2.30}$$

We know that is must satisfy the solvability condition

$$\lim_{T\to\infty} \frac{1}{T} \int_0^T \int_{\mathbb{R}} [u_1 R_u + v_1 R_v + p_1 R_p]\, dy\, dt = 0. \tag{2.31}$$

We note that that $u_1 f_{1\theta}$ terms are off frequency, so we need not worry about them. I also note that specifically for the Yanai wave $u_1 = p_1$ meridionally so $\int_{\mathbb{R}} u_1 v_2 u_{1y} + p_1 (v_2 p_1)_y dy = 0$ via integration by parts, so these terms should also be zero. The solvability condition from this problem is the NLS equation

$$iF_\tau + \frac{1}{2}\omega'' F_{\theta\theta} + \nu |F|^2 F = 0, \tag{2.32}$$

where $\omega'' = -\frac{1}{4}$, in agreement with Boyd, and $\nu \approx 0.3666$. We note that this may have also been attempted using the Hilbert transform directly as was done in Sine-Gordon, but the methods are equivalent.

We note that our ν differs with that Boyd finds ($\nu \approx 0.03$) with both waves present. Fundamentally however, the sign of the two coefficients are of opposite sign, so no solitons can form, in agreement with Boyd. Therefore we can say that this does not provide an explanation for the noted peak in the long Yanai wave. This result, while describing the MRG wave, also applies to the EIG0 wave via the aforementioned substitution $F \to D^*$.

2.4. Conclusion and Future Directions

We have considered the long time asymptotics of a pair of unidirectional dispersive problems. In both of these cases, the dispersion presents itself in the asymptotics in some version of the Nonlinear Schrodinger equation. This coincidence is not particularly surprising when we reconsider the equation at the heart of our analysis

$$u_{tt} + u = 0. \tag{2.33}$$

This equation has three solutions bases, whose differences come down to the types of data to dictate the initial conditions. The first is $\sin(t)/\cos(t)$, which best describes pointwise initial positions and derivatives. Next is e^{it}, e^{-it}, which naturally separates data by the sign of their frequency. The new pair $e^{t\mathcal{H}}, e^{-t\mathcal{H}}$, which separates data by the sign of phase velocity. However, these are all interchangeable via the linear complex structure given by i and $\mathcal{H}[]$, and the use of Euler's identity consequent of that structure. With this common structure, given the resonance present in both sinusoidal and complex exponential solutions, it should be of little surprise that the same resonances arise in the new basis.

Of pure mathematical interest, questions remain about the regularity of the solutions to the asymptotic equations. The Hilbert transform is a singular integral, and is unbounded on $L^1(\mathbb{R}), L^\infty(\mathbb{R})$. The products in the nonlinearities would also not necessarily preserve the regularity of the factors. For practical interests, in the periodic domain used in equatorial waves, any bounded solution will be in L^2, a space in which the Hilbert transform defined via the Fourier series is bounded.

This is not to say that the Hilbert transform cannot be used to create resonance dictated by a fundamentally new asymptotic equation. When Boyd conducted his research, he found that nondispersive, weakly dispersive, and strongly dispersive waves' asymptotics were described by the Burgers', (M)KdV, and NLS equations respectively. For unidirectional waves, [**Biello and Hunter, 2010**] studied the nondispersive case to find new asymptotics, and we studied the strongly dispersive case to find the the NLS variant. There could be an analog for the weakly dispersive case, but further research would be necessary to find an example.

CHAPTER 3

Instability via Meridional Circulation

3.1. Motivation

In the study of atmospheric dynamics, interactions between atmospheric waves and mean flows are an important aspect of characterizing the properties of each, for example their stability. While zonal mean flows have been the focus of extensive research, much less has been said regarding meridional/vertical background flow. This is an important consideration in the deep tropics, where the mean zonal flow vanishes, and since the velocities and their corresponding spatial derivatives tend to have inverse relative magnitudes, the velocities of all directions are equally important for transport [**Biello and Majda, 2010**].

Our work is to understand the effects of meridional circulation on equatorial waves, continuing that work done by [**Back and Biello, 2018**]. The major change that we relax the long wave approximation (i.e. $\partial_t, \partial_x, v \to 0$ uniformly), thus allowing the possibility of dispersion and instability. We consider both what happens in the shallow water equations, as well as the primitive equations.

3.2. Shallow Water Model

We begin with the shallow water equations

$$u_t + uu_x + vu_y - \beta yv + gh_x = \hat{F}^u - \hat{d}u, \tag{3.1a}$$

$$v_t + uv_x + vv_y + \beta yu + gh_y = \hat{F}^v - \hat{d}v, \text{ and} \tag{3.1b}$$

$$h_t + ((H+h)u)_x + ((H+h)v)_y = \hat{Q} - \hat{d}_\theta h. \tag{3.1c}$$

Here u, v are the zonal and meridional velocities, g is the gravitational constant H, h are the mean and perturbation geopotential heights, β is the meridional gradient of the Coriolis force, $\hat{d}$ is the drag, and $\hat{d}_\theta$ is the mass damping term. We can rescale h by g to define the gravity wave speed $c^2 = gH$, from which we can make the equations dimensionless by using the time scale $1/\sqrt{c\beta}$ and

length scale $\sqrt{c/\beta}$ in the horizontal directions, H in the vertical, which becomes

$$u_t + uu_x + vu_y - yv + h_x = F^u - du, \tag{3.2a}$$

$$v_t + uv_x + vv_y + yu + h_y = F^v - dv, \text{ and} \tag{3.2b}$$

$$h_t + ((1+h)u)_x + ((1+h)v)_y = Q - d_\theta h, \tag{3.2c}$$

where $d, d_\theta = \hat{d}, \hat{d}_\theta/\sqrt{c\beta}$.

3.2.1. Instability. We consider perturbations around a simple meridional background flow, where $u = \epsilon u, v = V(y) + \epsilon v, h = \epsilon h$, for a small ϵ. At $O(1)$ we get the following forcing balance

$$-yV = F^u, \quad VV_y = F^v, \text{ and } V_y = Q. \tag{3.3}$$

The zonal and height balances can be thought of as a particular instance of those found in equation (2.10) of [**Majda and Klein, 2003**]. Since we are investigating the role of meridional flow in (a) shallow water (b) in the full spectrum, we assume all of these are met.

At $O(\epsilon)$, we obtain the following linear PDEs

$$u_t + Vu_y - yv + h_x = -du, \tag{3.4a}$$

$$v_t + (Vv)_y + yu + h_y = -dv, \text{ and} \tag{3.4b}$$

$$h_t + (Vh)_y + u_x + v_y = -d_\theta h. \tag{3.4c}$$

It is easy to note that all of the non-advective terms on the left side form a skew self-adjoint system of equations. We show that $V\partial_y f + \frac{V_y}{2} f$ is skew self-adjoint by

$$\begin{aligned}\int_{-\infty}^{\infty} g\left(Vf_y + \frac{V_y}{2} f\right) dy &= gVf|_{-\infty}^{\infty} + \int_{-\infty}^{\infty} -(gV)_y f + g\frac{V_y}{2} f dy, \\ &= -\int_{-\infty}^{\infty} \left(g_y V + g\frac{V_y}{2}\right) f dy,\end{aligned}$$

given that either V or the solutions vanish as $|y| \to \infty$, which we take. While none of the advective terms are skew self-adjoint in themselves, the addition of $\pm\frac{V_y}{2}$ along the diagonals as appropriate on both sides will produce a self-adjoint system plus a diagonal system.

To show what how this can affect the dynamics, we consider the simple circulation $V = \alpha y$. While this is unbounded in y, our primary consideration is the deep tropics, where this is a reasonable approximation. Using $V_y = \alpha$, we compute the particular system

$$\begin{bmatrix} \partial_t + \alpha y \partial_y + \alpha/2 & -y & \partial_x \\ y & \partial_t + \alpha y \partial_y + \alpha/2 & \partial_y \\ \partial_x & \partial_y & \partial_t + \alpha y \partial_y + \alpha/2 \end{bmatrix} \begin{bmatrix} u \\ v \\ h \end{bmatrix} = \begin{bmatrix} -(d - \alpha/2)u \\ -(d + \alpha/2)v \\ -(d_\theta + \alpha/2)h \end{bmatrix}. \tag{3.5}$$

The left matrix is skew self-adjoint. The key quality of a skew-self adjoint operator is that for solutions of the form $\exp[ikx + \lambda t]$, with $\lambda := \mu - i\omega$, will have $\mu = 0$ for all k. However, the right hand side introduces self-adjoint terms to the system, which naturally controls μ. As a result, the circulation strength and damping ultimately control the statility of the system. A negative definite diagonal matrix is a sufficient condition to ensure stability. Applied to this damping matrix, this gives us a sufficient condition

$$\max\{-d, -d_\theta\} < \frac{\alpha}{2} < d. \tag{3.6}$$

For this a realistic circulation, we require that $\alpha > 0$, which make the lower inequality seem redundant, however, this condition generalizes for a generic circulation $V(y)$, which requires that over all y, we satisfy.

$$\max\{-d, -d_\theta\} < \frac{V_y(y)}{2} < d. \tag{3.7}$$

This entails that the stability of a system can, and will be spatially dependent.

As an example, if we consider the more realistic $V = \alpha y e^{-y^2/2}$, then $V_y = \alpha(1 - y^2)e^{-y^2/2}$. To guarantee stability (a) near the equator and (b) in the tropics (V_y is minimized at $y = \pm\sqrt{3}$,) we must satisfy

$$\max\{-d, -d_\theta\} < \frac{\alpha}{2} < d, \text{ and} \tag{3.8a}$$

$$-d < \frac{\alpha}{e^{3/2}} < \min\{d, d_\theta\}, \tag{3.8b}$$

respectively (for reference $e^{3/2} \approx 4.48$). Using [**Lin et al., 2005**, **Biello and Majda, 2010**] to estimate the values of $d \approx 0.07, d_\theta \approx 0.023$, we would ensure stability (a) near the equator with $-0.046 < \alpha < 0.14$, and (b) away from it with $-0.31 < \alpha < 0.1$.

While the condition is sufficient for stability, it is not necessary. Numerical computation of the eigenvalues finds that stability depends on the amplitude and structure of the circulation, and the particular modes themselves.

The first observation is that the sufficient condition held. Damping lowered the growth rates of these modes a consistent amount between the two models (see the top versus bottom rows of Figure 3.1). Another observation is that the growth rate of each mode exhibits a symmetry in the growth rate against α, which arises naturally from the symmetry under the transformation $\alpha \to -\alpha, t \to -t$ for the dragless scenario.

A more interesting observation is that the structure of the circulation affects the stability of the different modes. For example, with a purely linear circulation $V = \alpha y$, all modes observe $\frac{d\mu}{d\alpha} > 0$, so that increasing α decreases the stabilizing effects of circulation, whereas with the Hermite circulation the Kelvin wave and some others observe $\frac{d\mu}{d\alpha} < 0$ (see Figure 3.1).

Furthermore, it can be observed that the structure of the circulation affects the meridional structure of the modes in themselves. For example, in the Hermite circulation we observe a phase lag in the Kelvin wave for the subtropical regions where V_y is negative, observed consistently in Figures 3.2-3.4.

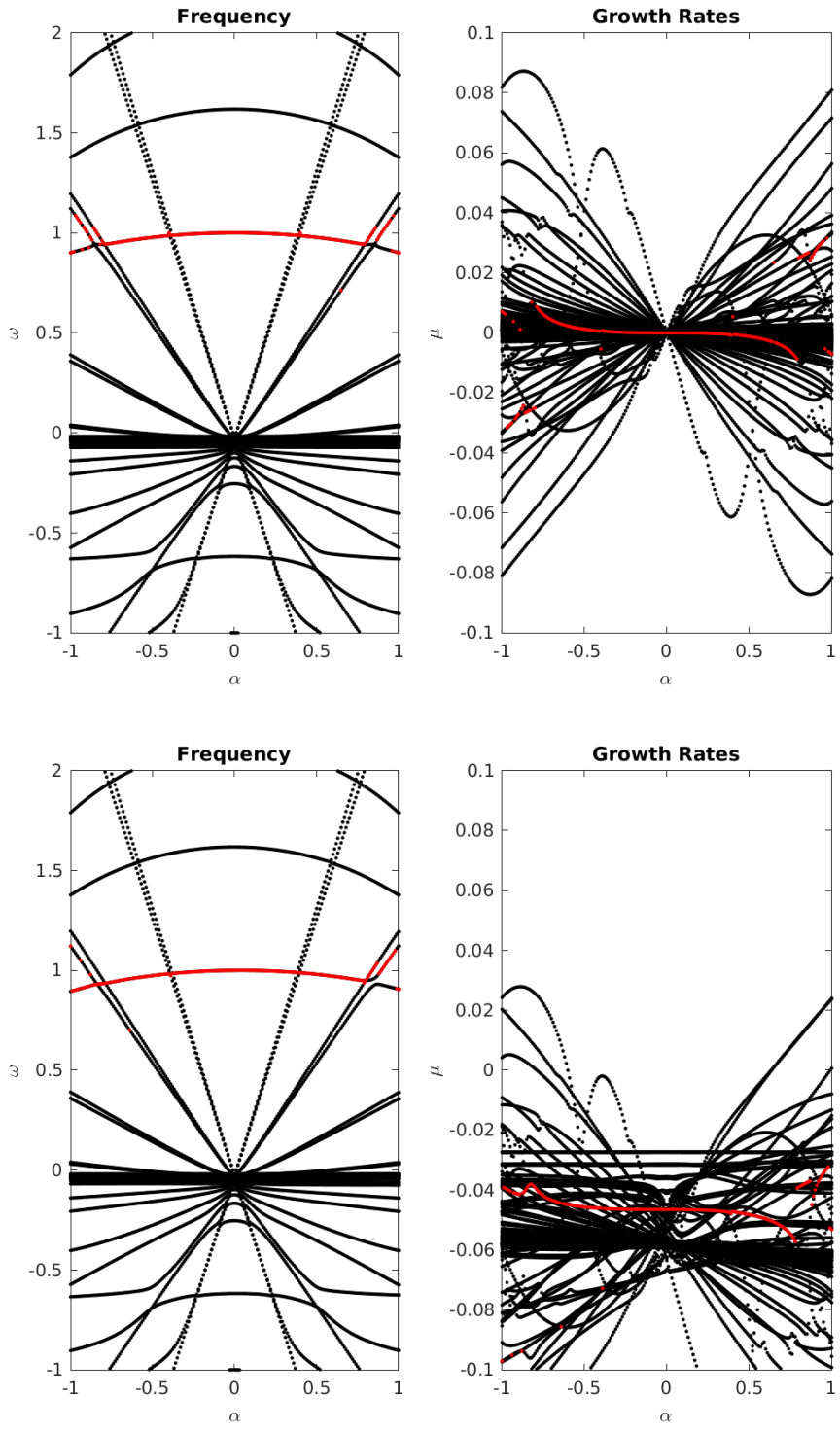

FIGURE 3.1. Eigenvalues in their components for the various modes at $k = 1$ (a fairly representative value) over a range of α values. Top row: no drag; Bottom row: $d = 0.07, d_\theta = 0.023..$ $V = \alpha y e^{-y^2/2}$. The red represents a greedy attempt at finding the Kelvin mode.

3.2.2. Damping Configurations. One important factor taken into account was the relative damping values. If we make the assumption that the circulation is driven by heating, i.e. $\alpha > 0$, we get that the stability condition (3.8b) reduces to

$$\alpha < \min\{2d, e^{3/2}d_\theta, e^{3/2}d\} \tag{3.9}$$

Each of the possibilities corresponds to a location of instability, and term that is primarily excited by this change. The $2d$ option corresponds to the excitation of zonal momentum at the equator, the $e^{3/2}d_\theta$ option to the height off the equator, and the $e^{3/2}d$ option to the meridional momentum off the equator.

The zonal momentum condition will always fail before the meridional momentum, but the height condition might fail before, between, or after both of these. We examine each of these in turn, using the value $d = 0.07$ in all cases. Thermal damping will fail first when $d_\theta < 2e^{-3/2}d \approx 0.031$, as happens using the previous numbers. Zonal momentum damping fails first when $2e^{-3/2}d < d_\theta < d$. The third case has thermal damping failing after both momenta dampings, here $d < d_\theta$. In this setup, we find that the growth rates decrease as d_θ increases, as expected. In addition, we find the Kelvin waves structure to mostly stay the same when varying d_θ, see Figures 3.2, 3.3, and 3.4. The one exception to this is the structure of relative potential vorticity $\zeta = -u_y - yh + v_x$.

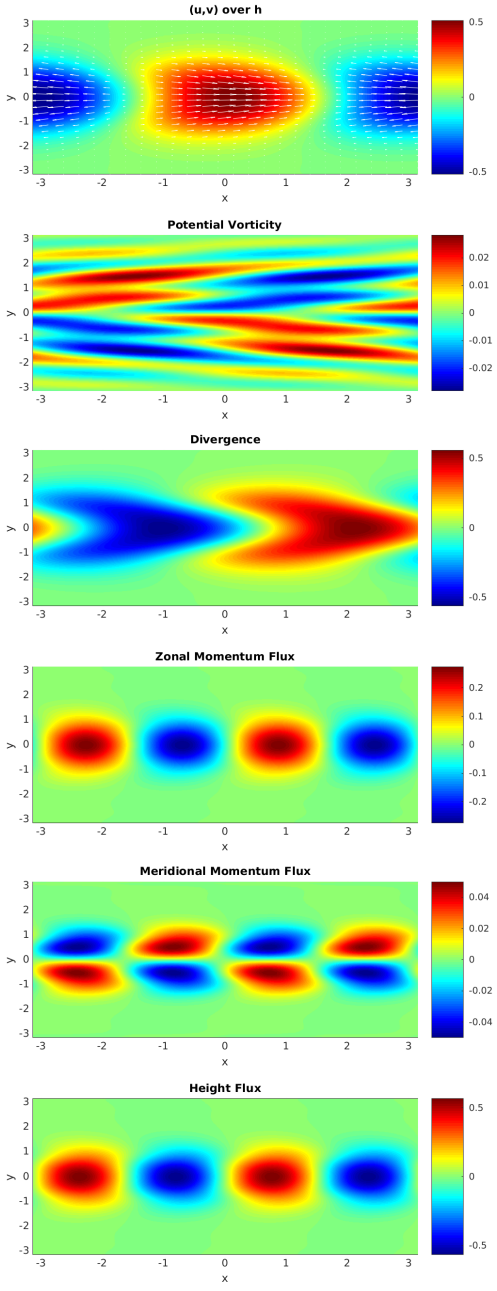

FIGURE 3.2. A presentation of the Kelvin mode for $d = 0.07, d_\theta = .023, \alpha = 0.5, k = 1$. This has a growth rate of -0.05. The momenta fluxes $-uu_x - uv_y$ and $-uv_x - vv_y$, and the height flux $-(uh)_x - (vh)_y$ represent the upscale nonlinear contributions produced by these waves.

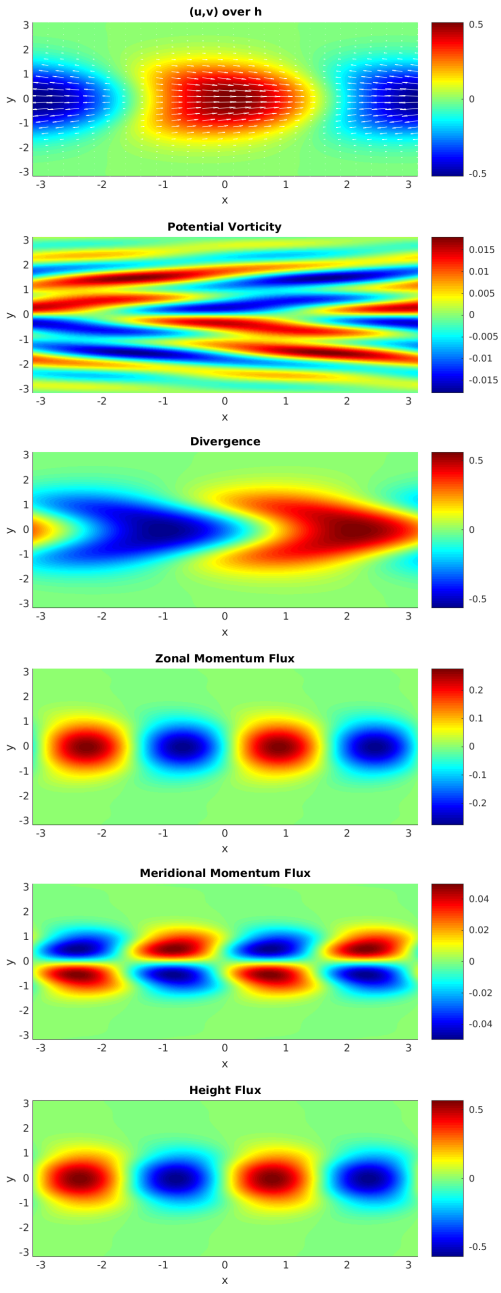

FIGURE 3.3. A presentation of the Kelvin mode for $d = 0.07, d_\theta = .046, \alpha = 0.5, k = 1$. This has a growth rate of -0.06.

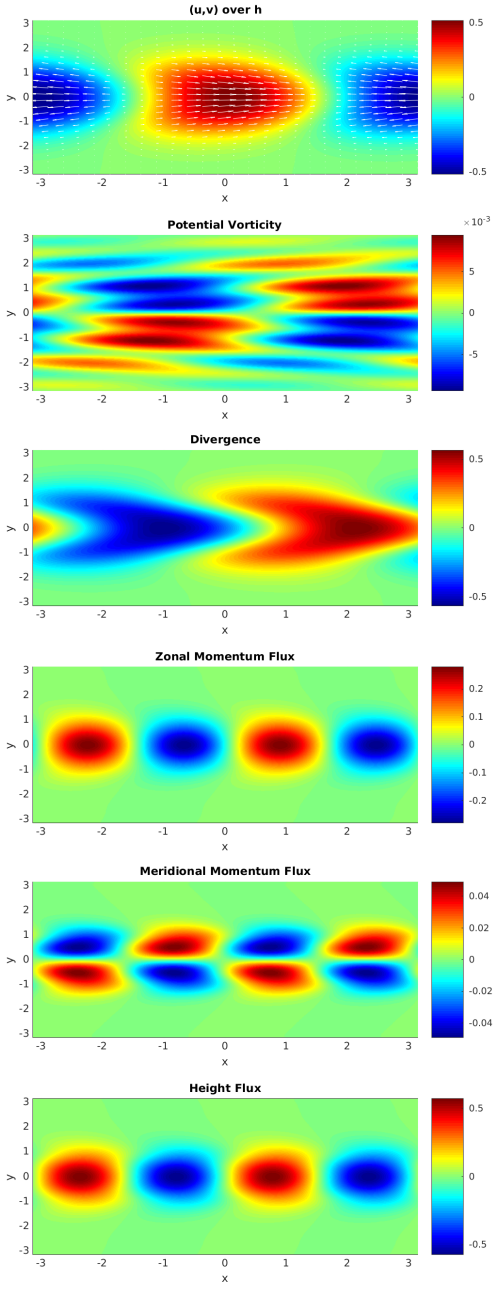

FIGURE 3.4. A presentation of the Kelvin mode for $d = 0.07, d_\theta = .092, \alpha = 0.5, k = 1$. This has a decay rate of -0.08.

3.3. Primitive Equation Model

The term V_y that characterizes shallow water instability also shows up in equation (18) of [**Back and Biello, 2018**], who use $|\omega| = \frac{1}{2}|V_y(y^*)|$ as a frequency cutoff for non-singular solutions of a reduced version of their problem, where the vanishing point of V defines y^*. The nature of this coincidence produces similar consequences, the larger V_y is, the higher the minimum frequency/drag needs to be for solutions to exist/remain stable. The big distinction though is that the breakdown in [**Back and Biello, 2018**] manifests itself in the meridional structure of the function, whereas here the problems manifests itself in time.

In order to conduct a proper comparison, it is necessary to repeat this analysis on the primitive equations. We note that [**Back and Biello, 2018**] uses the IMMD equations [**Biello and Majda, 2010**] as their starting point, which is a long wave model built on the primitive equations. One important difference in using the full primitive equations is that we relax the previous assumption of meridional geostrophic balance.

We now begin our computation with the primitive equations,

$$u_t + uu_x + vu_y + wu_z - yv + p_x = D^u, \tag{3.10a}$$

$$v_t + uv_x + vv_y + wv_z + yu + p_y = D^v, \tag{3.10b}$$

$$p_z - \theta = 0, \tag{3.10c}$$

$$u_x + v_y + w_z = 0, \text{ and} \tag{3.10d}$$

$$\theta_t + u\theta_x + v\theta_y + w\theta_z + w = S^\theta. \tag{3.10e}$$

Where D^u, D^v, S^θ are the dissipation and heating source the system. We expand the each field in the system $F(y,z) + \epsilon f(x,y,z,t)$, again with ϵ small. Filling out the expansion, at $O(1)$ we get the

mean equations,

$$VU_y + WU_z - yV = D^u, \tag{3.11a}$$

$$VV_y + WV_z + yU + P_y = D^v, \tag{3.11b}$$

$$P_z - \Theta = 0, \tag{3.11c}$$

$$V_y + W_z = 0, \text{ and} \tag{3.11d}$$

$$V\Theta_y + W\Theta_z + W = S^\theta. \tag{3.11e}$$

At $O(\epsilon)$ and using $\vec{u} = (u, v, w), \vec{U} = (U, V, W)$ to denote the velocity vectors, we get the anomaly equations,

$$u_t + \vec{u} \cdot \nabla U + \vec{U} \cdot \nabla u - yv + p_x = 0, \tag{3.12a}$$

$$v_t + \vec{u} \cdot \nabla V + \vec{U} \cdot \nabla v + yu + p_y = 0, \tag{3.12b}$$

$$p_z - \theta = 0, \tag{3.12c}$$

$$u_x + v_y + w_z = 0, \text{ and} \tag{3.12d}$$

$$\theta_t + \vec{u} \cdot \nabla \Theta + \vec{U} \cdot \nabla \theta + w = 0. \tag{3.12e}$$

Computing the energy of the anomaly, we find that it is not conserved,

$$\begin{aligned} &\frac{\partial}{\partial t}\left(\frac{1}{2}(u^2 + v^2 + \theta^2) + (uU + vV + \theta\Theta)\right) = -\nabla \cdot (\vec{u}P + \vec{U}p + \vec{u}p) + ... \\ &-\nabla \cdot \left(\vec{U}\frac{1}{2}(u^2 + v^2 + \theta^2) + \vec{u}\frac{1}{2}(U^2 + V^2 + \Theta^2) + \vec{U}(uU + vV + \theta\Theta)\right) + ... \\ &+uD^u + vD^v + \theta S^\theta - u(\vec{u} \cdot \nabla U) - v(\vec{u} \cdot \nabla V) - \theta(\vec{u} \cdot \nabla \Theta), \end{aligned} \tag{3.13}$$

with the nonconservative terms residing on the bottom line. We naturally expect drags and heat fluxes to play some role in adding or removing energy, so we make no further comment. The other non conservative terms are that way as a consequence of the linearization, had the nonlinear $\vec{u}\nabla v$ term been included, it would produce the conserved $\nabla \cdot (\vec{u}(vV) + \vec{u}\frac{1}{2}(v^2))$. An identical argument follows for the u, θ terms. As such, this linearized system is non-conservative. Of these non-conservative terms, $-v(\vec{u} \cdot \nabla V)$ is the most significant for our analysis of the role of meridional circulation, which does not appear in [**Back and Biello, 2018**] due to the long wave approximation,

where V, v scale with x, y. By contrast, the other two non-conservative terms are ignored because they are not part of a meridional circulation.

From here we begin using a Fourier expansion in the vertical direction, with $u, v, p = \phi_0 + \sum_n \phi_n \cos(nz)$, and $\theta, w = \sum_n \phi_n \sin(nz)$. At this stage we have taken that $\Theta = 0, P = 0, U = 0$, leaving us with $V = 2V(y)\cos(z), W = -2V_y(y)\sin(z)$, scaled to obtain simpler coefficients. This will satisfy the following simplified version of (3.11)

$$W = S^\theta \tag{3.14a}$$

$$V_y + W_z = 0 \tag{3.14b}$$

We expand (3.12) and split by vertical terms, using trigonometric product identities. For $\cos(nz), \sin(nz)$, we get the incompressibility and hydrostatic balance respectively for all $n \geq 1$

$$w_n = -\frac{1}{n}(u_{nx} + v_{ny}), \text{ and} \tag{3.15a}$$

$$p_n = -\frac{1}{n}\theta_n, \tag{3.15b}$$

which will be used fill in the dynamical equations such that the uncoupled system is skew self-adjoint. Expanding the remaining three equations will highlight the coupling between the vertical modes. We start with the barotropic equations,

$$u_{0t} - yv_0 + p_{0x} + (Vu_1)_y = 0 \tag{3.16a}$$

$$v_{0t} + yu_0 + p_{0y} + 2(Vv_1)_y + Vu_{1x} = 0 \tag{3.16b}$$

$$u_{0x} + v_{0y} = 0. \tag{3.16c}$$

Since it is incompressible, we can use a streamfunction $u_0 = -\psi_y, v_0 = \psi_x$ to simplify this to one equation by taking the curl of the momentum equation to get

$$\Delta\psi_t + \psi_x = (Vu_1)_{yy} - (Vu_1)_{xx} - 2(Vv_1)_{xy}. \tag{3.17a}$$

We continue the first baroclinic mode, and get

$$u_{1t} - yv_1 - \theta_{1x} = V\psi_{yy} - Vu_{2y}, \tag{3.17b}$$

$$v_{1t} + yu_1 - \theta_{1y} = -(V\psi)_{xy} - (Vv_2)_y + Vw_2, \text{ and} \tag{3.17c}$$

$$\theta_{1t} - u_{1x} - v_{1y} = -V\theta_{2y}. \tag{3.17d}$$

For higher baroclinic modes $n \geq 2$, we get the equations

$$u_{nt} - yv_n - \frac{1}{n}\theta_{nx} = -Vu_{n-1,y} - Vu_{n+1,y}, \tag{3.17e}$$

$$v_{nt} + yu_n - \frac{1}{n}\theta_{ny} = -(Vv_{n-1})_y - (Vv_{n+1})_y + V(w_{n+1} - w_{n-1}), \text{ and} \tag{3.17f}$$

$$\theta_{1t} - \frac{1}{n}u_{1x} - \frac{1}{n}v_{1y} = -V\theta_{n-1,y} - V\theta_{n+1,y}. \tag{3.17g}$$

The equations in (3.17) can then be simplified further by projecting onto the Fourier modes $\exp(i(kx - \omega t))$, which in essence replaces derivatives $\partial_x \to ik, \partial_t \to -i\omega$ for time and the zonal direction, and onto the Hermite functions (see Appendix A) in the meridional direction. This allows for these systems to be evaluated using spectral methods.

3.3.1. Instability. We start by examining the results for a small number (up to three) of vertical baroclinic modes, so that it might be compared to the longwave analysis done by [**Back and Biello, 2018**]. One major change is that our system is no longer skew self-adjoint. We will consider the profile given by [**Back and Biello, 2018**], $V = \alpha y e^{-y^2/2}$.

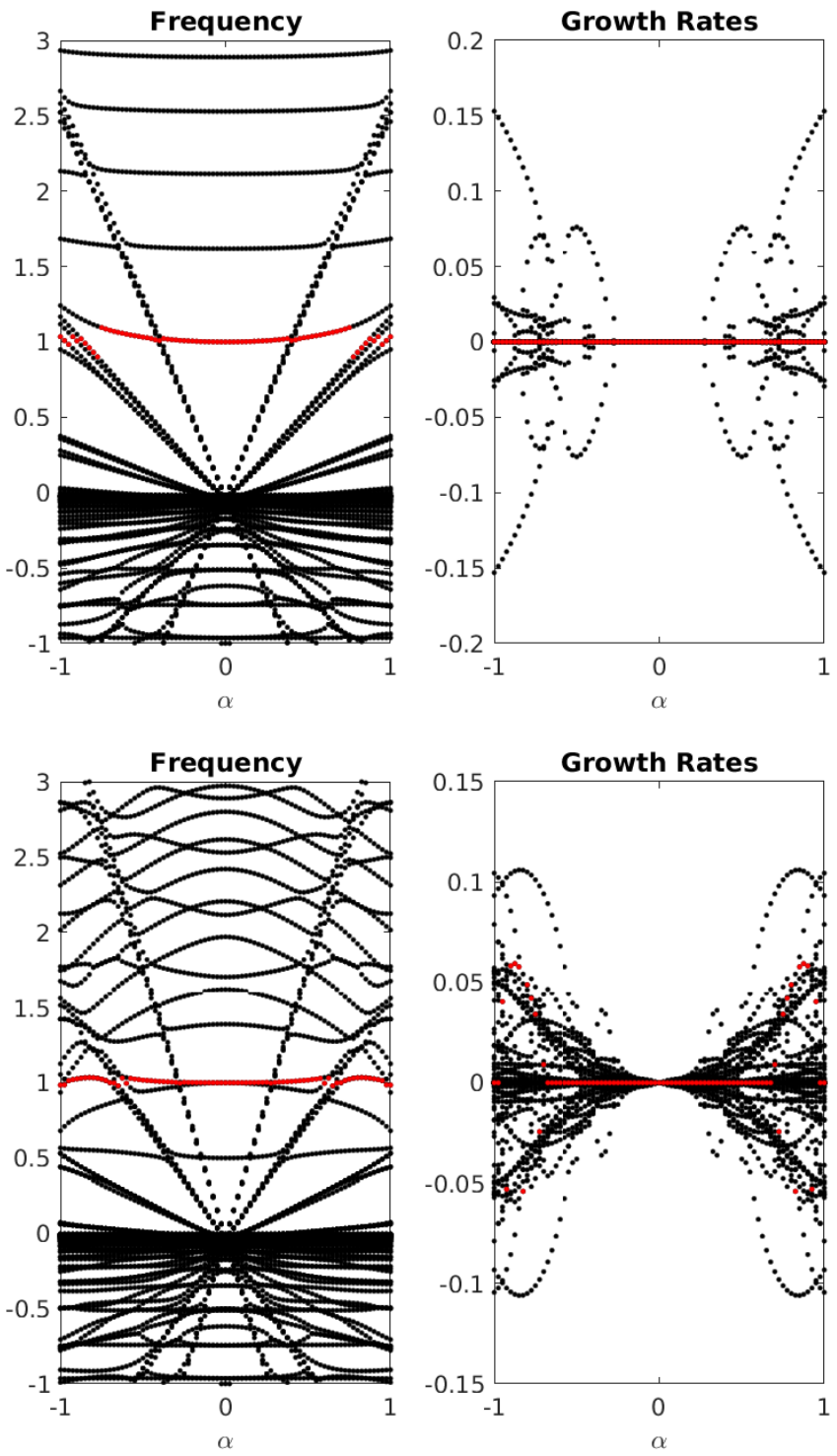

FIGURE 3.5. Eigenvalues in their components for the various modes at $k = 1$ (a fairly representative value) over a range of α value, for $V = \alpha y e^{-y^2/2}$. The top truncates to the first baroclinic mode, the bottom to the third. The red represents the a poor guess at finding the Kelvin mode. Here we do not observe instability for the Kelvin wave.

We also see instability varying with α, though it is much sparser compared to that observed in the shallow water equations. Of particular interest when trying to compare to [**Back and Biello, 2018**] and the shallow water equations is that the the Kelvin wave does not exhibit any growth rate, even a modest one as seen in the shallow water equations. This is seen eigenvalue plot in Figure 3.5, but was also verified by simulating the effects of a Kelvin wave initial condition.

We observe a four-fold symmetry in the growth rates, in that if (μ, α) appears in the plot, then all of $(\pm\mu, \pm\alpha)$ must as well, when compared to the shallow water equations, where we would only expect to see $(-\mu, -\alpha)$ on the plot.

We do see an increase in the number of unstable horizontal modes as we increase the vertical resolution. This hypothetically suggests that the mechanism of this instability presents itself in vertical transfers of energy, and that increasing the vertical resolution will reveal the instability in full.

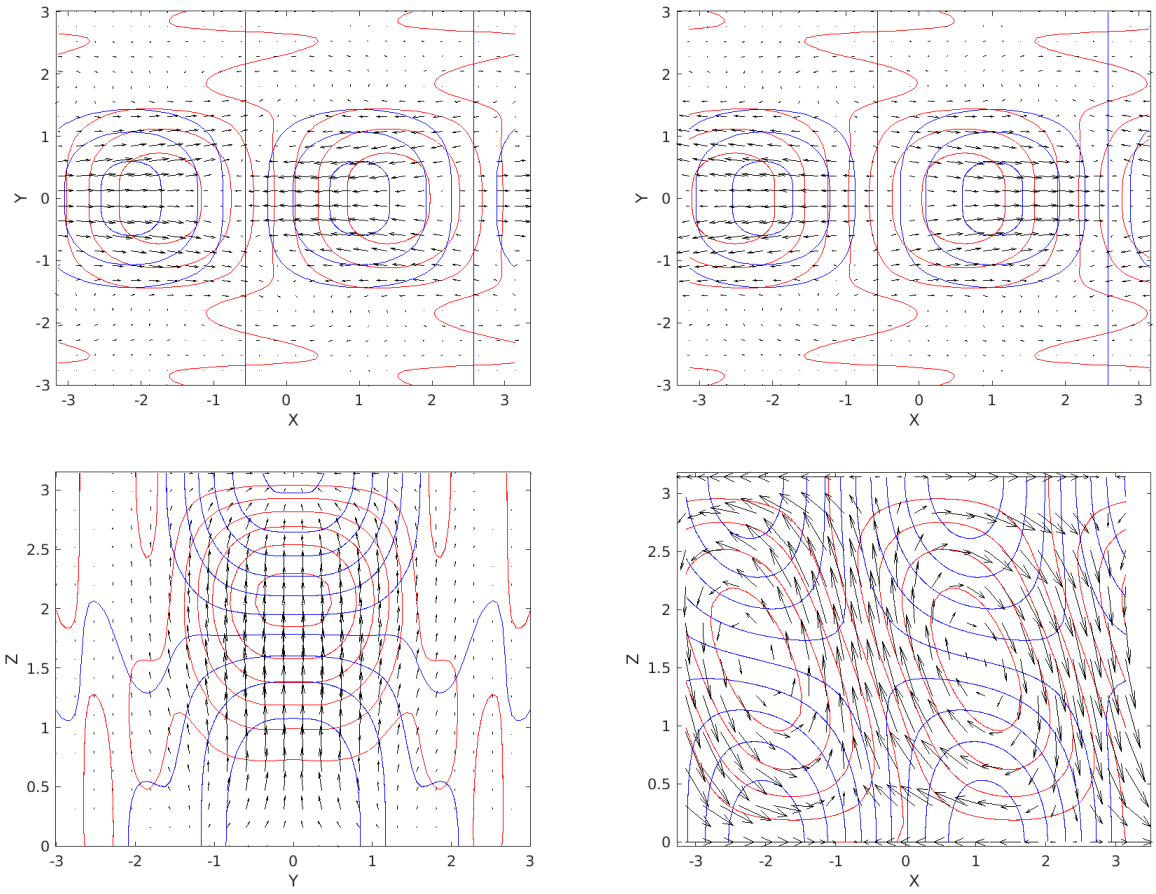

FIGURE 3.6. Slices of the Kelvin mode when $k = 1, \alpha = 0.5$ for two vertical baroclinic modes. Upper left: 750mb. Upper right: 250mb. Lower left: $x = 0$. Lower right: equator. Arrows indicate the winds in the slice, red contours isotherms, blue contours isobars.

3.4. Discussion

We find that the introduction of meridional circulation possesses a necessary condition for instability to the shallow water equation, as it breaks the skew self-adjointness of that algebraically ensures neutral stability. The meridional convergence V_y was found to be the key value for determining instability in the shallow water equations, which was previously found to cut off the physically viable solutions in the skew self-adjoint long-wave primitive equations [**Back and Biello, 2018**].

This break from skew self-adjointness naturally occurs in both the shallow water equations and the synoptic-scale primitive equations. However, in the latter case, we only observe the instability for a subset of the eigenmodes. Understanding this discrepancy merits further investigation.

CHAPTER 4

Extratropical Excitation of Equatorial Waves

4.1. Motivation

Convectively coupled equatorial waves play an important role in the control of tropical precipitation. The horizontal properties and dispersion of these waves are first unified in [**Matsuno, 1966**] from the linear theory of the equatorial shallow water equations. A full review of these waves and many of the complexities that arise from them can be found in [**Kiladis et al., 2009**] and references therein.

Our primary consideration is the response of the equatorial waves to a moving momentum forcing and diabatic heating in the extratropics. Significant milestones in this consideration were the response to stationary diabatic heating in [**Gill, 1980**], and the equatorial Kelvin response to forcing within an extratropical storm track found by [**Hoskins and Yang, 2000**]. Other studies examine the role of the subtropical jets, such that extratropical Rossby waves would interact with the equator via shear flow to produce unstable an Kelvin mode [**Sakai, 1989**, **Wang and Xie, 1996**, **Xie and Wang, 1996**, **Back, 2017**, **Barpanda et al., 2023**].

Our objective is to understand this extratropical connection as a response to a moving forcing. It is similar in many regards to [**Hoskins and Yang, 2000**], however they prescribe the frequency and wavenumber of the forcing and analyze the nonlinear response; we opt to instead use group velocity and wavenumber and look at the linear response. While these are significant changes, it allows us to isolate an equatorial Kelvin response to an extratropical forcing, depending solely upon the group velocity.

4.2. Shallow Water

We begin with full linearized shallow water equations in the equatorial β-plane, and with a forcing moving at a fixed latitude a with zonal phase velocity s, in an atmosphere with drag

coefficient d_u and thermal damping term d_θ.

$$\partial_{t'} u - \beta y v + \partial_{x'} p = F^u \delta(x' - st')\delta(y - a) - d_u u \tag{4.1a}$$

$$\partial_{t'} v + \beta y u + \partial_y p = F^v \delta(x' - st')\delta(y - a) - d_u v \tag{4.1b}$$

$$\partial_{t'} p + c^2[\partial_{x'} u + \partial_y v] = H\delta(x' - st')\delta(y - a) - d_\theta p \tag{4.1c}$$

Since this problem is linear, we only need to consider one s without loss of generality. This allows us to move to coordinates $x = x' - st', t = t'$ using a Galilean transform. We nondimensionalize the problem using β and the speed scale $c = 50\text{m s}^{-1}$ to the length scale $\sqrt{c/\beta} = 1500$ km and time scale $1/\sqrt{c\beta} = 8.3$ hr. We note that a wave with wavenumber 1 on a planetary scale corresponds to a wavenumber of about 0.03 in this system. This yields the system

$$(\partial_t - s\partial_x)u - yv + \partial_x p = F^u \delta(x)\delta(y - a) - d_u u \tag{4.2a}$$

$$(\partial_t - s\partial_x)v + yu + \partial_y p = F^v \delta(x)\delta(y - a) - d_u v \tag{4.2b}$$

$$(\partial_t - s\partial_x)p + \partial_x u + \partial_y v = H\delta(x)\delta(y - a) - d_\theta p \tag{4.2c}$$

We can rephrase the problem using the Riemann invariant $q = \frac{1}{\sqrt{2}}(u + p), r = \frac{1}{\sqrt{2}}(u - p)$ and ladder operators $\mathcal{L}^\pm = \frac{1}{\sqrt{2}}(\partial_y \pm y)$. We also introduce drag $D = \frac{d_u + d_\theta}{\sqrt{2}}, d = \frac{d_u - d_\theta}{\sqrt{2}}$.

$$(\partial_t + (1 - s)\partial_x)q + \mathcal{L}^- v = \frac{1}{\sqrt{2}}[F^u + H]\delta(x)\delta(y - a) - Dq - dr, \tag{4.3a}$$

$$(\partial_t + (-1 - s)\partial_x)r - \mathcal{L}^+ v = \frac{1}{\sqrt{2}}[F^u - H]\delta(x)\delta(y - a) - Dr - dq, \text{ and} \tag{4.3b}$$

$$\mathcal{L}^+ q - \mathcal{L}^- r + (\partial_t - s\partial_x)v = F^v \delta(x)\delta(y - a) - d_u v. \tag{4.3c}$$

We then project the equations meridionally onto the orthonormal basis of Hermite functions $\phi_m(y) = \frac{1}{\sqrt{m! 2^m \sqrt{\pi}}} H_m(y) e^{-y^2/2}$, (see Appendix A for details), then onto the Fourier mode $e^{ikx - i\omega t}$ in the zonal direction to the zonal wavenumber k and in frequency ω. Since the forcing does not change in t, the response will also be steady in time. For all $m \geq 0$, we obtain the linear problem

in q_m, r_{m-2}, and v_{m-1},

$$(1-s)ikq_m - \sqrt{m}v_{m-1} = \frac{F^u + H}{\sqrt{2}}\phi_m(a) - Dq_m - dr_m, \tag{4.4a}$$

$$(-1-s)ikr_{m-2} - \sqrt{m-1}v_{m-1} = \frac{F^u - H}{\sqrt{2}}\phi_{m-2}(a) - Dr_{m-2} - dq_{m-2}, \text{ and} \tag{4.4b}$$

$$\sqrt{m}q_m + \sqrt{m-1}r_{m-2} - sikv_{m-1} = F^v\phi_{m-1}(a) - d_u v_{m-1}. \tag{4.4c}$$

Terms with negative subscripts (e.g. r_{-2}) are omitted. We denote the full problem using the short hand $(L - iskI)z = F$, where z is the state vector, F is the forcing, I is the identity, and L encapsulates all the remaining terms in the system, including any drag. We consider solutions $(\hat{s}, \hat{z})$ to the eigenvalue problem problem $(L - i\hat{s}kI)\hat{z} = 0$, which is dependent on k. If there is no drag, the system is skew-Hermitian, which implies that $\hat{s}$ must be real, and the modes be neutrally stable. In the presence of drag, we compute the stability by examining the Fourier projection in the inertial reference frame

$$e^{ikx} = e^{ik(x' - \hat{s}t')} = e^{ik(x - \Re[\hat{s}]t)}e^{ik(-i\Im[\hat{s}]t)} \sim e^{k\Im[\hat{s}]t} \tag{4.5}$$

Throughout this, we have treated k as a parameter in the eigenvalue, so provided that $\hat{\omega} = k\Im[\hat{s}] < 0$, we will have stability. Unless otherwise specificed, we use damping values that come out from [**Lin et al., 2005**], $d_u = 0.07, d_\theta = 0.023$. We will have complex $\hat{s}$ eigenvalues, however the system is stable, see Figure 4.1.

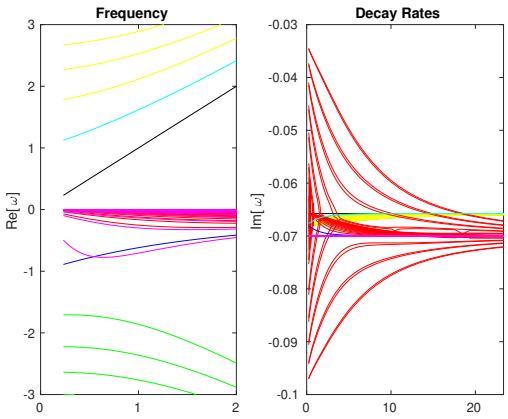

FIGURE 4.1. Left: The frequency wavenumber relation of the computed eigenmodes for the damped system, which examines the real part, and qualitatively matches [**Matsuno, 1966**] in the waves. We note that this dispersion relation captures both the barotropic (magenta) and baroclinic (red) Rossby waves. Right: The imaginary component of frequency over wavenumber. We note that it is negative everywhere, indicating a stable system, and is centered about the d_u, which is the stronger, save the behavior of the baroclinc Rossby wave. Both start at the lowest wavenumber $k_{min} = 0.2334$

4.2.1. Forcing Response. This section will assume that $d = 0$, which consequently decouples the shallow water equations into the blocks seen in Equation (4.4c). For each block, we can compute the forcing response $\phi_F = (L - isk)^{-1}F$, since the system is decoupled and has a regular structure, we can obtain exact solutions for each block. The inverse of a matrix is often expressed with a factor of its determinant, which for each block is $(-ik)\Delta_m$ where $\Delta_m = s(k^2 + 2m - 1) - k^2 s^3 + 1$ is a speed version of the Matsuno dispersion relation. This indicates that if the source moves like an equatorial wave of the same speed and wavenumber, then the response will see a resonance, limited by the damping terms.

We begin by examining the solution for the Kelvin wave, which is

$$q_0 = \frac{1}{(1-s)ik + D}\frac{F^u + H}{\sqrt{2}}\phi_0(a). \tag{4.6}$$

This corresponds to a Green's function of the form

$$\frac{\sqrt{\pi}}{1-s}e^{-D|x|/(1-s)}\Theta((1-s)x)(F^u + H)\phi_0(a)e^{-y^2/2}. \tag{4.7}$$

We observe that when $s < 1$, the response will be to the east of the forcing, and it will be to the west when $s > 1$, which follows from its motion relative to a Kelvin wave.

However, our solution also tells us what must happen to cause resonance. First, we have the location of the forcing, which here is controlled by $\phi_0(a)$. Since ϕ_m all have Gaussian terms, anything that is too far away from the extrema of a particular ϕ_m will have less of a role. However, ϕ_m forms a complete basis of functions, which means that no matter the latitude of forcing, some basis function will be excited. In particular for the Kelvin wave being excited by ϕ_0, the maximum is at the equator, and it has inflection points at latitudes $y = \pm 1$, beyond which the response drops off super-exponentially.

The next factor are the types and strengths of the different forcings. As a consequence of the Riemann invariant, the important combination of forcings are the following: $(F^u + H)/\sqrt{2}, F^v$, and $(F^u - H)/\sqrt{2}$. The first is that which drives the Kelvin wave: a combination of zonal momentum forcing and diabatic heating promotes a response in the zonal momentum and pressure, which are the constituents of a Kelvin wave, among other waves. However, we can see the role all three can play by considering the dragless mixed Rossby-gravity response ($m = 1$),

$$\begin{bmatrix} q_1 \\ v_0 \end{bmatrix} = \frac{1}{k^2(s-1)s - 1} \begin{bmatrix} sik & -1 \\ 1 & (s-1)ik \end{bmatrix} \begin{bmatrix} \frac{F^u+H}{\sqrt{2}}\phi_1(a) \\ F^v\phi_0(a) \end{bmatrix}, \tag{4.8}$$

or the more general inertio-gravity and Rossby wave responses ($m \geq 2$),

$$\begin{bmatrix} q_m \\ r_{m-2} \\ v_{m-1} \end{bmatrix} = \frac{1}{\Delta_m} \begin{bmatrix} [k^2 s(s+1) - (m-1)]\frac{1}{ik} & \sqrt{m}\sqrt{m-1}\frac{1}{ik} & (s+1)\sqrt{m} \\ \sqrt{m}\sqrt{m-1}\frac{1}{ik} & [k^2 s(s-1) + m]\frac{1}{ik} & (s-1)\sqrt{m-1} \\ -(s+1)\sqrt{m} & -(s-1)\sqrt{m-1} & (1-s^2)ik \end{bmatrix} \begin{bmatrix} \frac{F^u+H}{\sqrt{2}}\phi_m(a) \\ \frac{F^u-H}{\sqrt{2}}\phi_{m-2}(a) \\ F^v\phi_{m-1}(a) \end{bmatrix}. \tag{4.9}$$

However, the most significant determinant of response to the forcing is the proximity of the velocity of the forcing to the resonance (i.e. how small $\Delta_m(s;k)$ is). The amplitude of a resonance excitation will be $O(D^{-1})$ for the decoupled case, as shown for the Kelvin wave, and as computed for the other waves, but omitted for brevity. For the Kelvin wave, we see this resonance uniformly in k as $s \to 1$, where as for the other waves, no uniform limit exists in k, s or ω. This uniform limit is particularly interesting, in that it implies that provided that the forcing moves at speed $s = 1$, it will excite the Kelvin wave.

The velocity of the forcing also impacts the response for non-Kelvin waves in appropriate limits. In the limit $k \to \infty$ for $s = \pm 1$, resonance will excite the appropriate inertio-gravity waves. Additionally as $k \to 0$ for finite s, the Rossby waves will be excited by resonance.

Another feature that appears from the matrices in Equations 4.8,4.9 is the relative phase of the different components, captured by factors of i. As such, the meridional forcing and velocity operate out of phase with the other variables, except when the meridional forcing acts on the meridional velocity.

In addition to the Kelvin response that arises from the resonance of $s = 1$, we also expect a localized response near the forcing. We project to the total computed response onto the computed eigenmodes of the linear system to get their components. The eigenmodes are then identified as the equatorial waves by the eigenvalue s. In particular, we setup a forcing that had a strong and consistent Kelvin resonance across many horizontal wavenumbers k. In the limit $k \to 0$, we observe strong Rossby wave activity, and as $k \to \infty$, we observe strong eastward gravity wave activity, see Figure 4.2. The response seems to be dictated in large part by which waves are closest in frequency to the Kelvin wave, as evidenced by the response of the EIG0 wave.

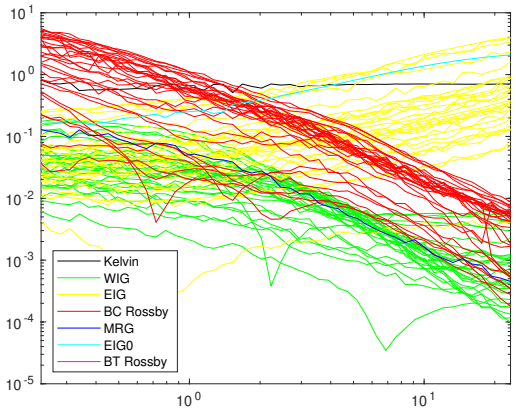

FIGURE 4.2. The inhomogeneous response to the forcing found in to the problem with $F^u = H = 1, s = 1$, located at $x = 0, y = 2.5$, with IPESD dampings $d_u = 0.07, d_\theta = 0.023$, over a range of horizontal wavenumbers k, starting with the lowest phyiscally acceptable value $k_{min} = 0.2334$. We observe a transition in the dominant response from being westward Rossby waves to eastward gravity wave, as well as the MRGs transition from gravity wave to Rossby wave. Since the activity is purely baroclinic, then we see no barotropic Rossby response.

We also note that the transition happens between the dominant response occurs at around $k = 1$, which implies that the response can be characterized by the aspect ratio of the zonal and meridional activity scales. The consequence of this is that in the longwave limit, we can expect appropriate subtropical forcing to both excite a Kelvin wave and Rossby waves.

4.3. Barotropic Interactions

One difference in the above work and much of the literature on Kelvin-Rossby phenomena is taking vertical motion into account somehow. As such, we examine the consequences of forcing the system in a system with barotropic and baroclinic activity, used in [**Majda and Biello, 2003**]. While this is a nonlinear equation, it seems like a possible avenue of investigation. This differs from the work in [**Back, 2017**] in that it investigates how the eigenmodes change as a result of a background jet with U_0 as an eigenvalue.

In the same units as above, we can define the two-layer equatorial β-plane equations for the barotropic and baroclinic horizontal velocity and pressure. We will denote the baroclinic terms using u, v, p as before, and the barotropic velocity will be represented by its streamfunction ψ. This will produce the system of equations

$$\partial_t \Delta\psi + \psi_x = F^{\omega} - J(\psi, \Delta\psi) - \nabla \cdot [(\vec{u}v)_x - (\vec{u}u)_y], \tag{4.10a}$$

$$\partial_t \vec{u} + y^{\perp}\vec{u} + \nabla p = F^{\vec{u}} - J(\psi, \vec{u}) - (\vec{u} \cdot \nabla)^{\perp}\nabla\psi, \tag{4.10b}$$

$$\partial_t p + \nabla \cdot \vec{u} = H - J(\psi, p), \tag{4.10c}$$

where $J(A, B) = A_x B_y - A_y B_x$ denotes the horizontal Jacobian ($J(\psi, \cdot)$ describes barotropic advective terms), and $^{\perp}$ denotes a quarter turn matrix $\begin{bmatrix} 0 & -1 \\ 1 & 0 \end{bmatrix}$. We note that for the usage of the stream function, we assert there is not barotropic heating. An immediate consequence of this derivation is that for barotropic momentum forcing $F^{\vec{v}_0}$, only the torque plays a role in forcing the system.

4.3.1. The Barotropic Rossby Problem. Before continuing, let us consider the barotropic linear response in isolation to forcing by solving the equation

$$\partial_{t'} \Delta\psi + \psi_{x'} = F^{\omega_0}\delta(x' - st')\delta(y - a). \tag{4.11}$$

We perform the Galilean transform as before, and again consider the steady state problem, which simplifies to

$$(1 - s\Delta)\psi_x = F^{\omega_0}\delta(x)\delta(y - a), \tag{4.12}$$

which is the Helmholtz equation when $s < 0$, and the screened Poisson equation when $s > 0$.From this, we can compute that the fundamental solution is

$$v_G = \psi_{x,G} = \frac{F^{\omega_0}}{s} \begin{cases} \frac{1}{2\pi} K_0(r/\sqrt{s}) & s > 0 \\ \frac{1}{4} Y_0(r/\sqrt{-s}) & s < 0 \end{cases} \tag{4.13}$$

where $Y_0, (K_0)$ is the (modified) Bessel function, and $r^2 = x^2 + (y - a)^2$ denotes the radius from the forcing point.

Strictly speaking, the full solution of the Helmholtz equation depends on the Hankel function $H_0 = J_0 + iY_0$, however, this is scaled by i, and we only take the real part. Furthermore as we approach the origin, we observe that the dominant balance of this equation is the Poisson equation, which behaves logarithmically there, so we expect in either case that the solutions here do the same, and J_0 is regular near the origin.

This results in an asymmetric behavior depending on the direction of the forcing. When the forcing moves westward, the solution oscillates away from the radius r, whereas the eastward solution exhibits strict decay.

4.3.2. Forcing via wave interaction. Suppose we have two real wave packets, traveling at phase velocity s_1 and s_2 at the same wavenumber k. Their product will be two waves, oscillating at the sum and difference of the wavenumber and speed. We compute that the wave travels at the average of the speeds at double the wavenumber.

$$e^{ik(x-s_1t)}e^{ik(x-s_2t)} = e^{2ik(x-\frac{s_1+s_2}{2}t)} \tag{4.14}$$

If we had a sufficiently fast eastward inertio-gravity wave (where $s > 1$ for all k) interacting with a barotropic Rossby wave (since the dispersion depends on meridional wavenumber l, which can be any real number), the forcing it produces could travel at the requisite speed $s = 1$, exciting a

Kelvin wave. This would not be found in [**Majda and Biello, 2003**] since they assume a long-wave approximation on Equation (4.10c), which filters out gravity waves.

For example, we'll consider the interaction between the barotropic Rossby wave and EIG0, which have dispersion relations

$$\omega_E = \frac{1}{2}\left(k + \sqrt{k^2+4}\right), \quad \text{and} \quad \omega_R = \frac{-k}{k^2+l^2} \quad \text{for } k > 0. \tag{4.15}$$

To resonantly excite a Kelvin wave, we must satisfy the following conditions

$$k_E + k_R = k_K, \text{ and}$$
$$\omega_E(k_E) + \omega_R(k_R) = \omega_K(k_K),$$

since the Kelvin wave is non-dispersive, this simplifies to the resonance relation

$$\frac{1}{2}(\sqrt{k_E^2+4} - k_E) = k_R\left(1 + \frac{1}{k_R^2+l^2}\right) \tag{4.16}$$

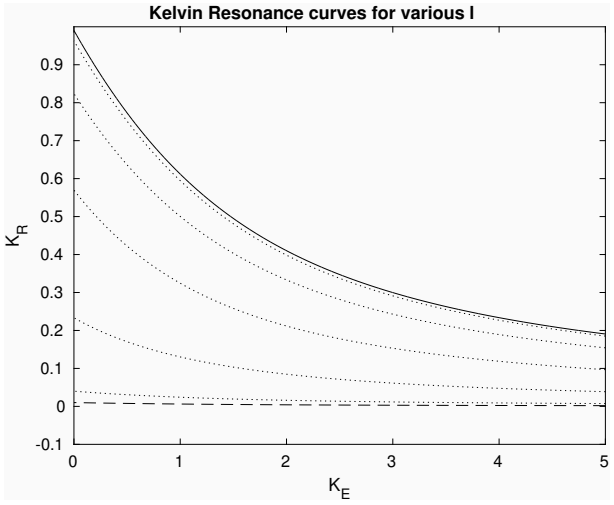

FIGURE 4.3. Plot of the resonance relation between k_E, k_R over various l, ranging from $l = 0.1$ (dashed line) to $l = 10$ (solid line).

We observer that solutions to this resonance relation cover the full spectrum in k_E, but only a finite bandwidth in k_R. What this implies is that essentially any gravity wave interacting with a long Rossby wave ($k_R < 1$, or whatever the maximum is for a specific l). If we think about this as vectors from the origin pointing at various points on the dispersion relations, the EIG and Kelvin

wave vectors will be pointing in roughly the same direction, that a small nudge from a Rossby wave can correct.

4.4. Conclusions

In summary, we find that activation of a Kelvin wave by forcing essentially depends upon producing a forcing that moves at the appropriate phase velocity. We also find a secondary response by Rossby or eastward inertio-gravity waves depending on the wavenumber of the forcing. In addition to generic forcing, we find that the nonlinear interaction between eastward inertio-gravity waves and long barotropic Rossby waves can also excite Kelvin waves.

APPENDIX A

Hermite Functions

Due to their ubiquity in my problems, I include the details of Hermite functions here. They are defined

$$\phi_m(y) = (2^n n!\sqrt{\pi})^{-1/2} H_m(y) e^{-y^2/2}, \tag{A.1}$$

where H_m is the "physicist" Hermite polynomial, defined as

$$H_m(y) = (-1)^m e^{x^2} \frac{d^m}{dx^m} e^{-x^2}. \tag{A.2}$$

The set $\{\phi_n\}_{n=0}^{\infty}$ are an orthonormal basis over $L^2(\mathbb{R})$ defined via the inner product $\langle f, g\rangle = \int_{\mathbb{R}} fg dy$. If we define the ladder operators $\mathcal{L}^{\pm} = \frac{1}{\sqrt{2}}(\partial_y \pm y)$, they satisfy the properties

$$\mathcal{L}^- \phi_m = -\sqrt{m+1}\phi_{m+1}, \quad \mathcal{L}^+ \phi_m = \sqrt{m}\phi_{m-1}. \tag{A.3}$$

Operating in this basis, these operators act as banded matrices. In particular

$$\hat{\mathcal{L}}^+ = \begin{bmatrix} 0 & \sqrt{1} & 0 & 0 & \cdots \\ 0 & 0 & \sqrt{2} & 0 & \cdots \\ 0 & 0 & 0 & \sqrt{3} & \cdots \\ 0 & 0 & 0 & 0 & \cdots \\ \vdots & \vdots & \vdots & \vdots & \ddots \end{bmatrix}, \hat{\mathcal{L}}^- = \begin{bmatrix} 0 & 0 & 0 & 0 & \cdots \\ -\sqrt{1} & 0 & 0 & 0 & \cdots \\ 0 & -\sqrt{2} & 0 & 0 & \cdots \\ 0 & 0 & -\sqrt{3} & 0 & \cdots \\ \vdots & \vdots & \vdots & \vdots & \ddots \end{bmatrix}, \tag{A.4}$$

and by linear combination, one can find the definitions of $y, \partial_y, \hat{y}$ (a symmetric matrix) and $\hat{\partial}_y$ (which is anti-symmetric). Thus we can compute the result of projections via the following formula for linear operators AB

$$\int_{\mathbb{R}} \phi_r(y)(AB\phi_c(y))dy = (\hat{A}\hat{B})_{rc} \tag{A.5}$$

The Hermite functions are also eigenfunctions of the Fourier Transform,

$$\frac{1}{\sqrt{2\pi}}\int_{-\infty}^{\infty} e^{ily}\phi_m(y)dy = i^m\phi_m(l) \tag{A.6}$$

This can also be used to project particular waves (e.g. a barotropic Rossby wave) onto the Hermite functions.

A.1. Primitive Equation Computations

As an example of how this works, we start with (3.17), truncated at $n = 1$, and apply the phase shift to $u_1, p_1 = -\theta_1$ by scaling by i, and express these in terms of Riemann invariants and ladder operators as before. We project the above equations on to the Hermite functions ϕ_m, which reduces to the system.

$$(k-\omega)q_{m+1} - \sqrt{m+1}v_m - \frac{1}{\sqrt{2}}\sum_n \gamma_{m+1,n}\psi_n = 0, \tag{A.7a}$$

$$(-k-\omega)r_{m-1} - \sqrt{m}v_m - \frac{1}{\sqrt{2}}\sum_n \gamma_{m-1,n}\psi_n = 0, \tag{A.7b}$$

$$-\sqrt{m+1}q_{m+1} - \sqrt{m}r_{m-1} - \omega v_m + k\sum_n \beta_{n,m}\psi_n = 0, \tag{A.7c}$$

$$-\frac{1}{\sqrt{2}}\sum_n (k^2\alpha_{n,m} + \gamma_{n,m})(q_n + r_n) - 2k\sum_n \beta_{n,m}v_n - [k + \omega k^2]\psi_m + \omega\sum_n \delta_{m,n}\psi_n = 0. \tag{A.7d}$$

During this projection, the coupling terms with V turn into integrals of a triad of these functions, which is a nontrivial operation that produces the coupling matrices $\alpha, \beta, \gamma, \delta$. These are defined $\alpha_{a,b} = \langle \phi_a, V\phi_b \rangle$, $\beta_{a,b} = -\langle \phi_a, V\partial_y\phi_b \rangle$, $\gamma_{a,b} = \langle \phi_a, V\partial_{yy}\phi_b \rangle$, $\delta_{a,b} = \langle \phi_a, \partial_{yy}\phi_b \rangle$. There calculation follows the principles above. Since the functions vanish as $|y| \to \infty$, integration by parts allows for the same matrices to be used multiple times.

Bibliography

[Back, 2017] Back, A. (2017). *Tropical Atmospheric Dynamics Modulated by Large-Scale Flows*. PhD thesis, UC Davis.

[Back and Biello, 2018] Back, A. and Biello, J. A. (2018). Effect of overturning circulation on long equatorial waves: A low-frequency cutoff. *Journal of the Atmospheric Sciences*, 75(5):1721–1739.

[Barpanda et al., 2023] Barpanda, P., Tulich, S. N., Dias, J., and Kiladis, G. N. (2023). The role of subtropical rossby waves in amplifying the divergent circulation of the madden–julian oscillation. *Journal of the Atmospheric Sciences*, 80(10):2377–2398.

[Battisti et al., 1999] Battisti, D. S., Sarachik, E., and Hirst, A. (1999). A consistent model for the large-scale steady surface atmosphericcirculation in the tropics. *Journal of climate*, 12(10):2956–2964.

[Bennett, 1976] Bennett, A. (1976). Open boundary conditions for dispersive waves. *J. Atmos. Sci.*, 33(2):176–182.

[Biello and Hunter, 2010] Biello, J. and Hunter, J. K. (2010). Nonlinear hamiltonian waves with constant frequency and surface waves on vorticity discontinuities. *Communications on pure and applied mathematics*, 63(3):303–336.

[Biello and Majda, 2004] Biello, J. A. and Majda, A. J. (2004). The effect of meridional and vertical shear on the interaction of equatorial baroclinic and barotropic rossby waves. *Studies in Applied Mathematics*, 112(4):341–390.

[Biello and Majda, 2010] Biello, J. A. and Majda, A. J. (2010). Intraseasonal multi-scale moist dynamics of the tropical atmosphere. *Communications in Mathematical Sciences*, 8(2):519–540.

[Boyd, 1980a] Boyd, J. P. (1980a). Equatorial solitary waves. part i: Rossby solitons. *Journal of Physical Oceanography*, 10(11):1699–1717.

[Boyd, 1980b] Boyd, J. P. (1980b). The nonlinear equatorial kelvin wave. *Journal of Physical Oceanography*, 10(1):1–11.

[Boyd, 1983a] Boyd, J. P. (1983a). Equatorial solitary waves. part 2: Envelope solitons. *Journal of Physical Oceanography*, 13(3):428–449.

[Boyd, 1983b] Boyd, J. P. (1983b). Long wave/short wave resonance in equatorial waves. *Journal of Physical Oceanography*, 13(3):450–458.

[Boyd, 1983c] Boyd, J. P. (1983c). Second harmonic resonance for equatorial waves. *Journal of Physical Oceanography*, 13(3):459–466.

[Chumakova et al., 2013] Chumakova, L. G., Rosales, R. R., and Tabak, E. G. (2013). Leaky rigid lid: New dissipative modes in the troposphere. *J. Atmos. Sci.*, 70(10):3119–3127.

[Edman and Romps, 2017] Edman, J. P. and Romps, D. M. (2017). Beyond the rigid lid: Baroclinic modes in a structured atmosphere. *J. Atmos. Sci.*, 74(11):3551–3566.

[Ekman, 1904] Ekman, V. W. (1904). On dead water. *Sci. Results Norw. Polar Expedi. 1893-96*, 5(15):152.

[Franklin, 1905] Franklin, B. (1905). *The writings of Benjamin Franklin*, volume 3. The Macmillan Company.

[Garner, 1986] Garner, S. T. (1986). A radiative upper boundary condition adapted for f-plane models. *Monthly weather review*, 114(8):1570–1577.

[Gill, 1980] Gill, A. E. (1980). Some simple solutions for heat-induced tropical circulation. *Quarterly Journal of the Royal Meteorological Society*, 106(449):447–462.

[Hoskins and Yang, 2000] Hoskins, B. J. and Yang, G.-Y. (2000). The equatorial response to higher-latitude forcing. *Journal of the atmospheric sciences*, 57(9):1197–1213.

[Kasahara and Qian, 2000] Kasahara, A. and Qian, J.-H. (2000). Normal modes of a global nonhydrostatic atmospheric model. *Monthly Weather Review*, 128(10):3357 – 3375.

[Khouider and Majda, 2006] Khouider, B. and Majda, A. J. (2006). Multicloud convective parametrizations with crude vertical structure. *Theoretical and Computational Fluid Dynamics*, 20:351–375.

[Khouider et al., 2012] Khouider, B., Majda, A. J., and Stechmann, S. N. (2012). Climate science in the tropics: waves, vortices and pdes. *Nonlinearity*, 26(1):R1.

[Kiladis et al., 2009] Kiladis, G. N., Wheeler, M. C., Haertel, P. T., Straub, K. H., and Roundy, P. E. (2009). Convectively coupled equatorial waves. *Reviews of Geophysics*, 47(2).

[Klemp and Durran, 1983] Klemp, J. B. and Durran, D. R. (1983). An upper boundary condition permitting internal gravity wave radiation in numerical mesoscale models. *Monthly Weather Review*, 111(3):430–444.

[Lin and Emanuel, 2022] Lin, J. and Emanuel, K. (2022). On the effect of surface friction and upward radiation of energy on equatorial waves. *Journal of the Atmospheric Sciences*, 79(3):837–857.

[Lin et al., 2005] Lin, J.-L., Zhang, M., and Mapes, B. (2005). Zonal momentum budget of the madden–julian oscillation: The source and strength of equivalent linear damping. *Journal of the atmospheric sciences*, 62(7):2172–2188.

[Lindzen, 2003] Lindzen, R. S. (2003). The interaction of waves and convection in the tropics. *J. Atmos. Sci.*, 60(24):3009–3020.

[Majda, 2003] Majda, A. (2003). *Introduction to PDEs and Waves for the Atmosphere and Ocean*, volume 9. American Mathematical Soc.

[Majda and Biello, 2003] Majda, A. J. and Biello, J. A. (2003). The nonlinear interaction of barotropic and equatorial baroclinic rossby waves. *Journal of the atmospheric sciences*, 60(15):1809–1821.

[Majda and Klein, 2003] Majda, A. J. and Klein, R. (2003). Systematic multiscale models for the tropics. *Journal of the Atmospheric Sciences*, 60(2):393–408.

[Majda et al., 1999] Majda, A. J., Rosales, R. R., Tabak, E. G., and Turner, C. V. (1999). Interaction of large-scale equatorial waves and dispersion of kelvin waves through topographic resonances. *Journal of the atmospheric sciences*, 56(24):4118–4133.

[Majda and Shefter, 2001] Majda, A. J. and Shefter, M. G. (2001). Models for stratiform instability and convectively coupled waves. *J. Atmos. Sci.*, 58(12):1567–1584.

[Marsico et al., 2023] Marsico, D. H., Biello, J. A., and Igel, M. R. (2023). Balanced convective circulations in a stratified atmosphere. part i: a framework for assessing radiation, the coriolis force, and drag. *Journal of the Atmospheric Sciences*, 80(12):2915–2924.

[Matsuno, 1966] Matsuno, T. (1966). Quasi-geostrophic motions in the equatorial area. *Journal of the Meteorological Society of Japan. Ser. II*, 44(1):25–43.

[Neelin and Held, 1987] Neelin, J. D. and Held, I. M. (1987). Modeling tropical convergence based on the moist static energy budget. *Monthly Weather Review*, 115(1):3–12.

[Purser and Kar, 2002] Purser, R. J. and Kar, S. K. (2002). Radiative upper-boundary conditions for a non-hydrostatic atmosphere. *Quarterly Journal of the Royal Meteorological Society*, 128(582):1343–1366.

[Raupp et al., 2019] Raupp, C. F. M., Teruya, A. S. W., and Silva Dias, P. L. (2019). Linear and weakly nonlinear energetics of global nonhydrostatic normal modes. *J. Atmos. Sci.*, 76(12):3831–3846.

[Rosales, 2003] Rosales, R. R. (2003). Weakly nonlinear expansions for breathers. `https://math.mit.edu/classes/18.306/Notes/Breathers.pdf`.

[Rudlosky and Fuelberg, 2013] Rudlosky, S. D. and Fuelberg, H. E. (2013). Documenting storm severity in the mid-atlantic region using lightning and radar information. *Monthly weather review*, 141(9):3186–3202.

[Sakai, 1989] Sakai, S. (1989). Rossby-kelvin instability: a new type of ageostrophic instability caused by a resonance between rossby waves and gravity waves. *Journal of Fluid Mechanics*, 202:149–176.

[Stein and Murphy, 1993] Stein, E. M. and Murphy, T. S. (1993). *Harmonic analysis: real-variable methods, orthogonality, and oscillatory integrals*, volume 3. Princeton University Press.

[Wang and Xie, 1996] Wang, B. and Xie, X. (1996). Low-frequency equatorial waves in vertically sheared zonal flow. part i: Stable waves. *Journal of Atmospheric Sciences*, 53(3):449–467.

[Xie and Wang, 1996] Xie, X. and Wang, B. (1996). Low-frequency equatorial waves in vertically sheared zonal flow. part ii: Unstable waves. *Journal of Atmospheric Sciences*, 53(23):3589–3605.

[Yano and Emanuel, 1991] Yano, J.-I. and Emanuel, K. (1991). An improved model of the equatorial troposphere and its coupling with the stratosphere. *Journal of Atmospheric Sciences*, 48(3):377–389.